Sodium Binding Interactions with the Aliphatic Amino Acids: A Guided Ion Beam and Computational Study

*Hanh D. M. Pham, Georgia C. Boles, and P. B. Armentrout**

Department of Chemistry, University of Utah, 315 S. 1400 E. Rm. 2020, Salt Lake City, Utah 84112, United States

ABSTRACT: Metal binding affinities play a vital role in medicinal, biological, and industrial applications. In particular, metal cation-amino acid interactions contribute to protein stability, such that analyzing analogous prototypical interactions is important. Here, we present a full description of the interactions of sodium cations (Na^+) and six aliphatic amino acids (AA), where AA = glycine (Gly), alanine (Ala), homoalanine (hAla), valine (Val), leucine (Leu), and isoleucine (Ile). Experimentally, these interactions are evaluated using threshold collision-induced dissociation carried out in a guided ion beam tandem mass spectrometer, allowing for the determination of the kinetic energy dependent behavior of Na^+–AA dissociation. Analysis of these dissociation cross sections, after accounting for multiple ion-molecule collisions, internal energy of reactant ions, and unimolecular decay rates, allows the determination of absolute Na^+–AA bond dissociation energies (BDEs) in kJ/mol of Gly (164.0), Ala (166.9), hAla (167.9), Val (172.7), Leu (173.7), and Ile (174.6). These are favorably compared to quantum chemical calculations conducted at the B3LYP, B3P86, MP2(full), B3LYP-GD3BJ, and M06-2X levels of theory. Our combination of structural and energetic analyses provides information regarding the specific factors responsible for Na^+ interactions with amino acids. Specifically, we find that the BDEs increase linearly with increasing polarizability of the amino acid.

Introduction

Alkali metal cation–peptide interactions play an important role in various biological systems.[1-6] In particular, sodium is a vital micronutrient present in extracellular fluid (ECF), which plays an important role in processes such as neuron function,[7-9] and osmoregulation[10] within the human body. Thus, our group and others have previously evaluated the sodium cation (Na^+) binding affinities to amino acids and other small organic systems,[11-25] where understanding the fundamental nature of these interactions is particularly useful because: (1) information obtained from the analysis of noncovalent alkali metal cation–peptide interactions enhances our understanding of their function in biological systems, and (2) it potentially allows for enhanced sequencing information regarding the location and coordination of the metal binding center. Similar structural and energetic analyses have been reported for additional alkali metal cations as well.[11-12,17-18,21,23-32]

In a continuation of such studies, we explore here the characteristics of akali metal cation binding to aliphatic amino acids (those that contain only carbon and hydrogen side chains, R) in order to elucidate binding affinities and key geometric information of interest. In particular, the systems of interest include Na^+(AA) complexes where AA = glycine (Gly, R = H), alanine (Ala, R = CH_3), homoalanine (hAla, R = CH_2CH_3), valine (Val, R = $CH(CH_3)_2$), leucine (Leu, R = $CH_2CH(CH_3)_2$) and isoleucine (Ile, R = $CH(CH_3)CH_2CH_3$). On a fundamental level, the examination of such small systems allows for a more complete understanding of the basic interactions between akali metal ions and amino acid residues and may also provide further insight regarding the metal ion affinity within a larger, more complicated sytem. Despite the small nature of these systems, however, careful consideration must be taken when determining the conformation and coordination of each complex.

In order to measure the bond dissociation energies (BDEs) of the Na^+(AA) complexes, their dissociation was evaluated using threshold collision-induced dissociation (TCID) carried out in a guided ion beam tandem mass specrometer (GIBMS). The kinetic energy dependent TCID cross sections were then modeled to yield experimental threshold energies that equal the 0 K BDEs

for the Na^+(AA) complexes. These experimental threshold values are then compared to theoretical BDEs obtained from quantum chemical calculations performed at B3LYP, B3P86, MP2(full), B3LYP-GD3BJ, and M06-2X levels of theory. In a complementary paper,[33] infrared (IR) spectra calculated at the B3LYP level are compared to IR multiple photon dissociation (IRMPD) spectra to ascertain the ground structures of all species. As demonstrated below, our experimental and theoretical analyses of these systems provide key information regarding the structural and energetic characteristics of the Na^+(AA) complex conformation and the noncovalent interactions.

Experimental and Computational Section

General Experimental Procedures

Kinetic energy dependent cross sections for the dissociation of Na^+(AA), where AA = Gly, Ala, hAla, Val, Leu, and Ile, with Xe were measured using a GIBMS that has been described in detail elsewhere.[34-36] Briefly, ions were generated via an electrospray ionization (ESI) source[37] using a solution of 10^{-4} M amino acid in 50:50 MeOH/H_2O and 10^{-3} M NaCl syringe-pumped at a rate of 0.35 μL/hr into a 35 gauge stainless steel needle biased at 2000 – 2900 V relative to ground. Ions were directed through a heated capillary at 80 °C into a radio frequency (rf) ion funnel,[38] where they were focused into a tight beam. After exiting the ion funnel, the ions entered a rf trapping hexapole ion guide where the ions underwent on the order of 10^5 thermalizing collisions with ambient gas. As demonstrated in earlier studies, ions produced in the source region should have a Maxwell-Boltzmann distribution of rovibrational states at 300 K.[19,37,39-41]

The precursor ions were extracted from the source and mass selected using a magnetic momentum analyzer, decelerated to a well-defined kinetic energy, and focused into a rf octopole ion guide that traps the ions radially,[34,42-43] which minimizes losses of product and reactant ions. The ions passed through a collision cell containing xenon[44-45] at a sufficiently low pressure (≤ 0.3 mTorr) such that the opportunity for multiple collisions to occur is minimal, although the number of ions undergoing single collisions is sufficient to produce product cross sections characterized by a high intensity. The product and remaining reactant ions drifted to the end of the octopole

guide, where they were extracted and focused into a quadrupole mass filter for mass analysis. Ions were detected with a high voltage dynode and scintillation detector,[46] and the signal was processed using standard pulse counting techniques. Ion intensities of reactants and products, measured as a function of collision energy, were converted to absolute cross sections as described previously.[34] Briefly, the calculation of the reaction cross section from ion intensities utilizes a relationship that is directly analogous to the Beer-Lambert Law, specifically, $I = I_0 \exp(-\rho\sigma l)$, where I is the reactant ion intensity after passing through the collision cell, I_0 is the reactant ion intensity entering the collision cell (taken to equal $I + I_P$, where I_P is the product ion intensity), l is the length of the collision cell (8.3 cm), and ρ is the number density of the neutral reactant and equals P/k_BT, where P and T are the pressure and temperature of the gas and k_B is Boltzmann's constant. The uncertainty in these relative cross sections is about ±5% and that for the absolute cross sections is about ±20%. The ion kinetic energy distribution was measured using a retarding potential analysis and found to be Gaussian with a typical full width at half maximum (FWHM) of 0.1 - 0.2 eV (lab). Uncertainties in the absolute energy scale are about ±0.05 eV (lab). Ion kinetic energies in the laboratory (lab) frame were converted to energies in the center-of-mass (CM) frame using $E_{CM} = E_{lab}\, m/(m + M)$, where M and m are the masses of the ionic and neutral reactants, respectively. All energies in this work are reported in the CM frame unless stated otherwise.

Thermochemical Analysis

Thresholds of the TCID cross sections were modeled using eq 1,

$$\sigma(E) = \sigma_0 \sum_i g_i (E + E_i - E_0)^n / E \quad (1)$$

where σ_0 is an energy-independent scaling factor, n is an adjustable, empirical representation of factors that describe the efficiency of the energy transfer during collision and varies with the complexity of the system being studied,[35] E is the relative kinetic energy of the reactants, E_0 is the threshold for dissociation of the ground electronic and rovibrational state of the reactant ion at 0

K. The summation is over the rovibrational states of the reactant ions, i, where E_i is the excitation energy of each state and g_i is the population of those states, ($\Sigma g_i = 1$). Vibrational frequencies and rotational constants were taken from quantum chemical calculations, as detailed in the following section. The Beyer–Swinehart-Stein-Rabinovitch algorithm[47-49] was used to evaluate the number and density of the rovibrational states and the relative populations g_i were calculated for a Maxwell-Boltzmann distribution at 300 K.

Data interpretation can be obscured by several systematic issues (primarily multiple reactant ion/neutral gas collisions and lifetime effects) that must be taken into account during analysis in order to produce accurate thermochemical data. An additional effect arises from the internal energy of reactant ions, which is included explicitly in eq 1. To ensure rigorously single collision conditions, data were collected at three different pressures, about 0.2, 0.1, and 0.05 mTorr, and the cross sections were extrapolated to zero pressure prior to analysis. Figure S1 shows example cross sections for the Na^+(Ile) system taken at these different pressures and the pressure extrapolated (0.0 mTorr) cross section, along with the thresholds found at each pressure. (Notably, modeling of the highest pressure cross section data results in a lower threshold, by about 0.14 eV in the example case). Secondly, dissociation of large molecules with many internal modes may not occur during the time scale of the experiment, $\sim 5 \times 10^{-4}$ s. This lifetime effect can produce an observed threshold with an onset delayed from the thermodynamic limit (a kinetic shift) that becomes more noticeable as the size of the molecule increases. These kinetic shifts are estimated by incorporating Rice-Ramsperger-Kassel-Marcus (RRKM) statistical theory,[50] which predicts the unimolecular rate of dissociation of an energized molecule, into eq 1, as described in detail elsewhere.[51]

In all complexes studied here, we assumed that the dissociation occurs via a loose transition state in the phase space limit (PSL) such that the transition states were assumed to be product like.[51-52] Thus, the transitional frequencies, those that become rotations of the completely dissociated products, were treated as rotors. The external rotational constants of the transition state (TS) were determined by assuming that the TS occurs at the centrifugal barrier for interaction of

Na^+ with the neutral amino acid, calculated as outlined elsewhere.[51-52] The 2-D external rotations were treated adiabatically but with centrifugal effects included, consistent with the discussion of Waage and Rabinovitch.[53] In the present work, the adiabatic 2-D rotational energy was treated using a statistical distribution with an average rotational energy, as described in detail elsewhere.[51,54] Overall, this PSL model has been shown previously to provide accurate estimation of kinetic shifts for CID processes involving alkali metal ions.[20,24,27,29-30,39,55-57]

The model cross sections of eq 1 were convoluted with the kinetic energy distributions of the reactants[34] and compared to the experimental data. A nonlinear least-squares analysis was used to provide optimized values for σ_0, n, and E_0. These threshold energies were converted to 0 K BDEs by assuming that E_0 represents the energy difference between reactants and products at 0 K. This requires that there are no activation barriers in excess of the endothermicity of dissociation.[58] The uncertainty in E_0 was estimated from the range of threshold values determined from multiple sets of data, variations in the parameter n (±10% around the optimum value), variations in vibrational frequencies (±10%), changes in the time available for dissociation by factors of 2, and the uncertainty in the absolute energy scale (0.05 eV, lab).

Computational Details

For all model structures, the Gaussian 09 suite of programs[59] was used in order to calculate vibrational frequencies and energies of the neutral and sodiated complexes of interest. Geometries for the neutral AAs and their sodiated complexes were initially optimized at the B3LYP/6-311+G(d,p) level.[60-62] In order to find the lowest energy conformers, all reasonable conformations were explored by systematically altering the side-chain dihedral angles. Possible sodium cation binding sites were directed by previous studies.[14,63-65] Vibrational frequencies (scaled by 0.989 when used in internal energy determinations or for RRKM calculations)[66] and rotational constants were calculated from these optimized structures. Single point energies were calculated at the B3LYP, B3P86, and MP2(full)/6-311+G(2d,2p)[67-68] level using the B3LYP/6-311+G(d,p) geometries. Additionally, geometry optimizations of low-lying species (using the 6-311+G(d,p)

basis set) and subsequent single point energies (using the 6-311+G(2d,2p) basis set) were performed at the B3LYP-GD3BJ[69-70] and M06-2X[71] levels of theory such that theoretical BDEs were also calculated at these levels of theory. Basis set superposition errors (BSSE) were estimated using the full counterpoise method at all levels of theory used in this work.[72]

Results

Cross Sections for Collision-Induced Dissociation

Experimental cross sections were obtained for the interaction of Xe with Na^+(Gly), Na^+(Ala), Na^+(hAla), Na^+(Val), Na^+(Leu), and Na^+(Ile). The only process observed at energies and pressures used in the current analysis is the loss of the intact neutral ligand via the collision-induced dissociation reaction 2.

$$Na^+(AA) + Xe \rightarrow Na^+ + AA + Xe \qquad (2)$$

Zero-pressure extrapolated cross sections for all six systems are shown in Figure 1. For all complexes, cross sections increase quickly from thresholds in the vicinity of 1.5 eV until about 4 eV, at which point the cross section levels off with magnitudes of $10 - 30 \times 10^{-16}$ cm^2. In a previous study of the Na^+(Gly) and related systems, a ligand exchange reaction forming $NaXe^+$ was additionally observed at higher energies.[14] In all cases, the maximum cross sections for $NaXe^+$ observed were at least two orders of magnitude smaller than the primary Na^+ product, which would be at the edge of the signal-to-noise level in the present experiments. We searched for the analogous process in the current study, although no such formation was observed.

Theoretical Results for Low-Energy Conformers

Neutral Ligands. Several low-energy conformers for each neutral amino acid were calculated as described above with results provided in Table 1. Different conformers are identified by their dihedral angles, designated as c (cis) for angles <50°, t (trans) for those >135°, and g (gauche) for all intermediate angles. In order to distinguish between otherwise identical names, + and − subscripts may also be given for some angles. Dihedral angles are measured starting from

the carboxylic acid hydrogen, and go to the lone pair (Lp) of electrons on the amino group for all six amino acids (∠HOCC$^{\alpha}$, ∠OCC$^{\alpha}$N, and ∠CC$^{\alpha}$NLp). For the five amino acids having a side chain longer than Ala, the side chain dihedrals are also given in parentheses as ∠CC$^{\alpha}$C$^{\beta}$C$^{\gamma}$ for homoalanine, ∠CC$^{\alpha}$C$^{\beta}$H for valine, ∠CC$^{\alpha}$C$^{\beta}$C$^{\gamma}$ and ∠C$^{\alpha}$C$^{\beta}$C$^{\gamma}$H) for leucine, and ∠CC$^{\alpha}$C$^{\beta}$C$^{\gamma}$ and ∠C$^{\alpha}$C$^{\beta}$C$^{\gamma}$C$^{\delta}$ for isoleucine.

All lower energy conformations were explored up to ~25 kJ/mol, which resulted in the location of about 10 conformers for the smallest Gly and Ala systems and 20 – 30 conformers for the larger hAla, Val, Leu, and Ile systems. For these latter systems, relaxed potential surfaces at the B3LYP/6-311+G(d,p) level of theory (to probe unique rotamers) were calculated to better explore conformational space. An overview of select low-energy conformers located for each system is given in Supporting Information Figures S2 – S7. Energies at select levels of theory for higher energy species are described in Tables S1 – S5.

Four glycine conformers were located within 7 kJ/mol of the Gly-ttt ground structure (GS), Table 1 and Figure S2. Here, ttt is characterized by ∠HOCC$^{\alpha}$, ∠OCC$^{\alpha}$N, and ∠CC$^{\alpha}$NLp angles of 180°, respectively, and two equivalent ∠CC$^{\alpha}$NH angles of 59°. Amino nitrogen hydrogens are oriented towards the carbonyl oxygen in a symmetric fashion with equivalent long-range NH•OC interactions of 2.84 Å. As shown in Table 1, the ccc conformer is low lying (1 – 7 kJ/mol above the GS) and characterized by a 1.94 Å OH•N hydrogen bond (and there are two enantiomers because ∠HOCC$^{\alpha}$ = ±1.35°). The ttg species adopts a similar conformation as the ttt GS, although the amino group is rotated such that there is only a single hydrogen bond of 2.39 Å between the amino group and carbonyl oxygen, NH•OC. The energetic cost associated with undergoing this rotation is about 5 kJ/mol. Higher energy tct, tcg, ctt, and ctg species were located 7 – 25 kJ/mol higher in energy than the GS, Tables 1 and S1 and Figure S2. These results are consistent with previous computational modeling of the glycine potential energy surface in the location of the global minimum and low-energy conformers.[14,73-76] In rare gas matrices, the ttt, ccc, and tct conformers have been identified using infrared spectroscopy, and it has been shown that tct converts to ttt upon annealing.[76-77] Further, the Gibbs energies at 358 K between ttt and ccc was

measured as 6.1 ± 0.6 kJ/mol and between ttt and tct as 5.5 ± 0.6 kJ/mol,[77] in reasonable agreement with the values calculated at the B3LYP, MP2, and M06-2X (although the latter predicts a 2.8 kJ/mol difference between ccc and tct) levels of theory but contrasting with the order predicted by the other two levels (Table 1).

B3LYP, B3LYP-GD3BJ, MP2, and M06-2X predict an Ala-ttt GS at both 0 and 298 K, whereas B3P86 suggests that a ccc species is lowest in energy at 0 K by 1.1 kJ/mol. Here, the ttt GS adopts a conformation similar to the glycine GS, where both amino hydrogens are oriented towards the carbonyl oxygen (Figure S3); however, the presence of the methyl group rotates the ∠OCC$^{\alpha}$N angle such that it deviates from 180° by 19°. Thus, the long-range NH•OC hydrogen bonds are characterized by different lengths, 2.69 and 2.94 Å. The ccc$_-$ and ccc$_+$ species correspond to the two ccc enantiomers of Gly, and will henceforth be designated as ccc$_A$ (for anti) and ccc$_S$ (for syn) indicating that the lone pair (and for the complexes, the sodium cation) lies on the opposite or same side as the side chain, respectively. These conformers lie within 1.3 kJ/mol of one another, and only 0.9 – 4.1 and 2.2 – 5.5 kJ/mol above the ttt GS at 0 and 298 K, respectively, for all levels of theory except B3P86. They are both characterized by a OH•NH$_2$ hydrogen bond (1.90_5 and 1.92 Å, respectively), nearly equivalent to that observed in the analogous glycine system. These two species are distinguished by the orientation of their amino hydrogens and therefore the ∠CC$^{\alpha}$NLp dihedral angles (-22° in ccc$_A$ and +23° in the ccc$_S$ species). Additional low-lying ttg$_-$, tg$_-$t, ttg$_+$ species (Figure S3) were located 5 – 7 kJ/mol higher in energy than the respective GS. Higher energy species are described in Table S1. Similar to the glycine system, our computational results are consistent with previous studies evaluating low-energy conformations of alanine.[78-80] Further, the jet-cooled microwave rotational spectra of Alonso and co-workers clearly indicates that the ttt conformer dominates by a factor of 3 to 4 over ccc$_S$,[79] consistent with the predictions of all levels of theory but B3P86 (Table 1). Similarly, IR spectra in rare gas matrices finds a 90:10 mixture of ttt and ccc$_S$.[81]

As for Ala, different levels of theory predict two different GSs for hAla (Table 1 and Figure S4). B3LYP, B3LYP-GD3BJ, MP2, and M06-2X suggest that the hAla-ttt(t) species is lowest in

energy, whereas B3P86 instead predicts that the ccc(t) conformer is the GS. The ttt(t) and ccc(t) conformers are equivalent to the ttt and ccc conformers of Gly and Ala, with the former stabilized by long-range (>2.59 and 3.04 Å) NH•OC interactions and the latter by an OH•N hydrogen bond (1.90 Å). In both of these conformers, the ethyl side chain points away from the rest of the molecule. If the side chain is rotated, one obtains the low-lying ttt(g_-) and ttt(g_+) species. Relative energies of these species are consistent with a theoretical analysis completed previously at the MP2/6-311++G(d,p) level.[82] Further, the jet-cooled microwave rotational spectra obtained by Blanco et al.[79] indicate that the GS is ttt(t) followed by ttt(g_-) and then ccc(t). B3P86 predicts the wrong GS, whereas B3LYP and B3LYP-GD3BJ invert the predicted order of the latter two conformers at 298 K. MP2 and M06-2X make predictions at 298 K that match the experimental order. An additional 17 higher energy structures were located and are described in Supporting Information Table S2 and Figure S4 for select structures.

B3LYP, MP2, B3LYP-GD3BJ (298 K) and M06-2X predict a Val-ttt(c) species where the amino hydrogens are oriented towards the carbonyl oxygen via long range interactions > 2.5 Å (Figure S5). B3LYP-GD3BJ (0 K) and B3P86 instead suggests the ccc(c_+) conformer is lowest in energy, where the amino nitrogen is hydrogen bound to the hydroxy hydrogen of the carboxylic acid via OH•N. Rotation around the ∠$CC^{\alpha}C^{\beta}H$ angle results in the location of two additional rotamers of each type. Here, ttt(g_-) and ttt(t) are 2 – 5 and 5 – 8 kJ/mol higher in energy than the ttt(c) GS, respectively. At similar energies, ccc_S(t) and ccc_A(t) rotamers are located about 5 and 10 kJ/mol above ccc(c_+), respectively. Select higher energy conformers are described in Supporting Information Table S3 and Figure S5. Similar theoretical results have been observed in previous studies on the conformation of neutral valine.[83-84] The jet-cooled rotational spectra of Alonso indicate that only ttt(c) and ccc(c_+) are formed experimentally (consistent with all levels of theory but B3P86), but suggest that conformational cooling may remove the higher energy ttt(x) and ccc(x) conformers.[83] Similarly, IR spectra in an Ar matrix also find a dominant ttt(t) ground state, with population of ccc(t) and a trace amount of tct(c), where conformational cooling of other low-lying conformers was believed to have occurred.[85]

All levels of theory except B3P86 at 0 K predict that the GS of Leu is ttt(tg_+), although this species lies only 0.8 kJ/mol above the B3P86 predicted GS, ccc(tg_+) (Figure S6). Similar to the other B3LYP predicted GSs, the amino hydrogens are oriented towards the carbonyl oxygen in ttt(tg_+). These interactions are slightly longer than in the smaller systems and are > 2.6 Å. Formation of the OH•N hydrogen bond in ccc(tg_+) is energetically favorable at the B3P86 level, although is 1.3 kJ/mol higher at 298 K and 0.2 – 6 kJ/mol higher in energy at the remaining levels of theory. Additional higher energy conformers located are included in Supporting Information Table S4 and Figure S6. Analogous results have been obtained previously from theory,[84,86-87] where the latter study included 150 different conformers as well as barriers separating them. Jet-cooled rotational spectra find ttt(tg_+) as the dominant conformer along with ccc(tg_+), where again conformational cooling may have removed higher lying ttt(xx) and ccc(xx) species.[86] In agreement, matrix isolation studies find the same two conformers with ttt(tg_+) dominating along with smaller amounts of ttt(g_-g_-).[87] Again conformational cooling was believed to occur in the rare gas matrices at 5 – 22 K.

Analogous GSs are observed in the Ile system, where B3LYP, MP2, B3LYP-GD3BJ (298 K) and M06-2X suggest that Ile-ttt(g_-t) is lowest in energy, whereas B3P86 and B3LYP-GD3BJ (0 K) instead predict ccc(g_-t). These two species are slightly more energetically competitive than in the smaller systems, lying within 3.5 kJ/mol. A description of higher energy Ile conformers is given in Table S5 and select conformers are shown in Figure S7. These results are consistent with previous computational studies,[84,88] and the jet-cooled rotational spectra reveal the presence of the ttt(g_-t) (dominant) and ccc(g_-t) conformers. IR spectra in a rare gas matrix located five conformers, which they identified as ILE1 = ttt(g_-t), ILE2 = ccc(tg_-), ILE3 = tg_+t(tt), ILE4 = ccc(g_-t), and ILE8 = tg_-t(tt), with a distribution of 88% txt(xx) and 12% ccc(xx).[89] Note that our conformers do not include ccc(tg_-) because this has the wrong stereochemistry at C^β (along with their ILE9 and ILE13) and hence should not have been included in their evaluation. Presumably, the identification of ILE2 in the IR spectrum needs to be replaced by another ccc type conformer. Nevertheless, the distribution of txt and ccc conformers should remain valid. This distribution is best predicted by

our M06-2X results (90 and 10%), although B3LYP and MP2 calculations yield reasonable results (79 and 21%). Boeckx et al. likewise concluded that MP2/6-31G(d,p) calculations were accurate, whereas B3LYP/6-31G(d,p) calculations were not, but the latter are improperly skewed by the low energy of the inaccurate ILE2 conformer.

Sodiated Complexes. Several low energy Na^+(AA) conformers were found for each amino acid. Relative 0 and 298 K energies for low-energy conformers (lowest four or all those <5 kJ/mol at the B3LYP level) are given in Table 2. Here, metal binding sites are designated in square brackets, followed by the amino acid dihedral angle orientation, as outlined in Figure 2. Metal binding sites are identified as the amino nitrogen (N), carbonyl oxygen (CO), hydroxy group (OH), or both oxygens of a carboxylate group (CO_2^-). Dihedral angles are again characterized as c, t, and g and specify $\angle HOC^1C^2$ and $\angle OC^1C^2N$, along with the same side chain designations described above in parentheses. Higher energy species are described in Tables S6 – S9 and Figures S8 – S10.

For the Na^+(Gly) system, a number of low-energy conformations are possible and have been examined in detail by Jensen,[63] Hoyau and Ohanessian,[64] Marino et al.,[65] Moision and Armentrout,[14] and to a lesser extent by Wyttenbach et al.[90] and Bouchonnet and Hoppilliard.[91] In all these studies, the GS is predicted to be the [N,CO]-tt structure, Table 2 and Figure 3, as also found here at all levels of theory. As in these previous works, another conformer of this binding type was also found, [N,CO]-ct. Structurally, these two conformers differ in the hydrogen orientation of the carboxylic acid, where the GS maintains a hydrogen bond between the hydroxy hydrogen and carbonyl oxygen. Loss of this hydrogen bond shifts the energy of the ct conformer 21 – 22 kJ/mol above the tt GS. Three other low-energy binding motifs were located, [CO], [CO_2^-] (a zwitterionic species), and [CO,OH]. Here, [CO]-cc, [CO_2^-]-cc and [CO,OH]-cc (Figure S8) lie 6 – 15, 7 – 19, and 6 – 14 kJ/mol above the GS at 0 K, respectively. (Note that the [CO_2^-] and [CO,OH] conformers lie in a double-well potential connected by proton motion between the N and O centers. The same connection holds for these two conformers for all six of the AAs considered here. Likewise, the [CO] and [CO,OH] conformers are connected by changing the CONa bond angle.) Hoyau and Ohanessian calculated the transition states for interconversion

among the various isomers.[64] Previous studies also located three other structures, [N,OH]-tc, which we calculate to lie 35 – 42 kJ/mol above the GS, and [CO]-tc and [CO]-tt, which we calculate to lie 48 – 53 and 50 –54 kJ/mol above the GS (Table S6 and Figure S8). Jensen did the most thorough analysis of possible Na^+(Gly) structures, locating 14 total (those already mentioned plus [N]-tt, [N]-tc, [N]-ct, [CO]-ct, and three structures where a hydrogen was moved from NH_2 to form a diol). These structures are not included here as they were calculated to lie >75 kJ/mol above the GS at the MP2/6-31G(d,)//HF/6-31G(d) level.[63] Although the presence of multiple conformers being present experimentally is unlikely given the relative energies found for these Na^+(Gly) systems, an equilibrium distribution of conformers at 298 K was calculated. Indeed, these results suggested that the [N,CO]-tt GS would have populations > 95% at most levels of theory (77% at B3P86).

We also point out one interesting nuance to the [N,CO]-tt GS structure that becomes important for the larger aliphatic amino acids; namely, because the NH_2 hydrogens try to avoid eclipsing the adjacent CH_2 hydrogens, the amino group rotates so that HCNH = ±24° and ±28°. This also shifts the Na^+ to one side or the other of the backbone. When the side chain R = H, these two structures are enantiomers; however, for more complicated R, the two structures have different energies resulting from weak interactions between Na^+ and the side chain, as discussed further below.

Similar to the glycine system, the Na^+(Ala) GS is predicted to adopt a [N,CO]-tt_+ conformation, Figure 3. As just noted, the addition of the methyl side chain now distinguishes the two enantiomers of Na^+(Gly), resulting in an additional low-energy [N,CO] complex, [N,CO]-tt_-, which lies only 1 – 3 kJ/mol higher in energy than the tt_+ GS. Notably, this subtle distinction was not commented on in previous theoretical work, which only located the tt_+ conformation.[65,92] The lower energy tt_+ conformer has the sodium cation on the same side of the backbone as the methyl side chain. To more clearly define this characteristic, throughout the rest of the paper, this conformer will be designated as tt_S (for syn), with the tt_- conformer called tt_A (for anti). For the case of Ala, we also located the transition state between these two conformers, finding that it lies

only 0.02 – 0.4 kJ/mol above the higher energy tt_A structure (1.8 – 3.5 kJ/mol above tt_S).

The lowest energy zwitterionic structure, Na^+(Ala)[CO_2^-]-cc (lying 0.7 – 14 kJ/mol above the GS at 0 K and 0.2 – 13 kJ/mol at 298 K) is lower in relative energy than the analogous Na^+(Gly) zwitterionic species. The related [CO,OH]-cc structure (Figure S8) lies ~5.8 kJ/mol above [CO_2^-]-cc at 0 K (3.2 – 4.6 at 298 K) except at the M06-2X level where it is lower by 0.5 (1.8) kJ/mol. The monodentate [CO]-cc structure now lies 2 – 5 kJ/mol above [CO,OH]-cc, Table S6. 298 K equilibrium populations of these low-lying species at the B3LYP, MP2, B3LYP-GD3BJ, and M06-2X levels were found to be 83 – 99% for the [N,CO]-tt_S and [N,CO]-tt_A, 0.3 – 15% for [CO_2^-]-cc, and 0.5 – 3% for [CO,OH]-cc conformers (58, 33, and 9% at the B3P86 level). Thus, it can be assumed that the dominant species formed in the source is [N,CO]-tt, consistent with previous results.[65,92]

At most levels of theory, the Na^+(hAla) GS adopts a [N,CO] configuration, although B3P86 suggests the [CO_2^-]-cc(t) species is the GS, Table 2 and Figure 3. B3LYP finds that [N,CO]-tt_S(t) is the GS, whereas MP2, B3LYP-GD3BJ, and M06-2X levels of theory instead predict [N,CO]-tt_S(g_-) is the GS. Indeed, as shown in Table 2, there are five low-lying [N,CO] geometries that differ in the orientation of the side chain or whether the sodium cation is syn or anti relative to the side chain, Figures 4 and S9. All levels of theory agree that the [N,CO] geometries are low-lying (<5 kJ/mol above the GS), whereas the [CO_2^-]-cc(t) and cc(g_-) conformers lie more than 6 kJ/mol above the GS at the B3LYP-GD3BJ and M06-2X levels. Our exploration of conformational space resulted in the location of 18 additional conformers lying >5 kJ/mol above the GS, as described in Supporting Information Table S6. Overall, one can expect a distribution of these conformers to be formed experimentally. Equilibrium populations at 298 K suggest that [N,CO] isomers dominate for B3LYP and MP2 (67 and 71%) and for B3LYP-GD3BJ and M06-2X (94 and 99%), whereas B3P86 indicates only 37%, with [CO_2^-] isomers occupying 47% (28, 25, 6, and 1% at the other levels of theory, respectively). The effect of multiple conformers being present experimentally is discussed below.

Different levels of theory suggest different GSs for Na^+(Val), Table 2. B3LYP and B3P86

predict a zwitterionic [CO_2^-]-cc(g_+) complex, whereas MP2, B3LYP-GD3BJ, and M06-2X instead predict a [N,CO]-$tt_S(g_+)$ structure, Figure 4. These two structures are within 1 kJ/mol of each other at the B3LYP and MP2 levels of theory, with the zwitterionic species lying 6 and 10 kJ/mol higher in energy than the charge solvated complex at the B3LYP-GD3BJ and M6-2X levels, respectively, and the reverse order by 3 kJ/mol for B3P86. These results agree with those of Lemoff et al. who found the [N,CO] structure was more stable by 1.7 kJ/mol at 298 K at the B3LYP/6-31++G(d,p) level.[93] As for hAla, we also located several low-lying [N,CO] structures differing in the syn/anti and side chain orientations, Table 2. These additional [N,CO] conformers were generally found to be lower in energy than additional zwitterionic species, Tables 2 and S7. [N,CO]-$tt_A(g_+)$, $tt_S(t)$, and $tt_S(g_-)$ (Figure S9) lie 1 – 4, 1 – 6, and 4 – 7 kJ/mol above the respective GSs. The next lowest energy zwitterionic complex, [CO_2^-]-cc(t) (Figure S9) was found 4 – 16 kJ/mol above the GSs. Table S7 lists an additional 17 higher energy structures. Given the prediction of multiple GSs, an equilibrium distribution of conformers at 298 K was explored here. Populations of 51, 67, 94, and 98% for [N,CO] and 37, 31, 6, and 1% for [CO_2^-] type structures are predicted at the B3LYP, MP2, B3LYP-GD3BJ, and M06-2X levels of theory, respectively. B3P86 again indicates the zwitterion is favored by 61% versus 30% for [N,CO] structures.

Most levels of theory suggest that Na^+(Leu)[N,CO]-$tt_S(tg_+)$ (Figure 4) is the GS at 0 K. At the B3P86 level, [CO_2^-]-cc(tg_+) was instead found to be lower in energy by <3 kJ/mol. This zwitterionic species is lower in energy than [N,CO]-$tt_S(tg_+)$ at 298 K by 0.3 kJ/mol at the B3LYP level, but 1 – 11 kJ/mol higher at MP2, B3LYP-GD3BJ, and M06-2X levels. These results are consistent with previous B3LYP/6-311++G(d,p) calculations that found the [N,CO] structure was lower in energy than [CO_2^-] by 2.6 kJ/mol at 0 K.[94] In addition, we located two other [N,CO] structures that were low lying (1 – 4 kJ/mol above the GS at all levels but B3P86 where the difference is 4 – 7 kJ/mol) along with [CO_2^-]-cc(tg_-), 3 – 14 kJ/mol above the GSs, Figure S10. Table S8 lists an additional 22 higher energy isomers. A 298 K equilibrium distribution would yield 56 – 99% [N,CO] and 1 – 40% [CO_2^-] except for B3P86, which predicts a 30 to 61% distribution.

Results for Na^+(Ile) are similar to those for Na^+(Leu). B3LYP and B3P86 suggest that the zwitterionic Na^+(Ile)[CO_2^-]-cc(g_t) structure is the 0 and 298 K GS (Table 2 and Figure 4), whereas B3LYP-GD3BJ and M06-2X instead predict that the charge solvated Na^+(Ile)[N,CO]-tt$_S$(g_t) is lower in energy (by 5 – 12 kJ/mol), Figure 4. MP2 predicts these structures are essentially isoenergetic. These two structures are analogous to those reported previously.[94] Again, we find three other low-lying structures for the charge solvated [N,CO] species lying 1 – 8 kJ/mol above the GSs at 298 K, and two additional zwitterionic structures lying 3 – 16 kJ/mol above the GSs, Figure S10. Table S9 lists an additional 27 higher energy isomers. An equilibrium population at 298 K of the different structures suggest 51 – 99% [N,CO] and 1 – 48% [CO_2^-] for most levels of theory, with B3P86 indicating a 28 to 70% distribution.

Spectroscopic results for Na^+(AA) Complexes

Previously, Kapota et al. had examined the infrared multiple photon dissociation (IRMPD) spectroscopy of Na^+(Gly).[95] They determined the spectrum from 1100 – 1850 cm^{-1} and found it was most consistent with the [N,CO]-tt structure. Recently, we have reexamined this system along with the Na^+(AA) complexes for AA = Ala, Val, Leu, and Ile over the spectral range of 500 – 1900 cm^{-1} using light from the free electron laser at the FELIX (Free Electron Lasers for Infrared eXperiments) facility at Radboud University in the Netherlands. These results are reported in detail elsewhere.[33] For Na^+(Gly), our results confirm those of Kapota et al. and can be interpreted by only the [N,CO]-tt GS, although minor contributions from other isomers cannot be spectroscopically eliminated in either study. For the other four complexes, the spectra indicate that the [N,CO] structures again dominate the species present but that contributions from [CO_2^-] structures are evident. These results are inconsistent with the prediction of B3P86 theory, which suggests that the zwitterionic species are the GS. They are also inconsistent with results from the B3LYP-GD3BJ and M06-2X calculations, which would predict little if any contributions at 298 K from the zwitterionic species. For all four of these amino acids, our B3LYP and MP2 calculations predict 298 K equilibrium distributions that favor the [N,CO] structures but also

include contributions from [CO_2^-] of 15, 37, 40, and 48% (B3LYP) and 15, 31, 29, and 36% (MP2). These predictions are consistent with the IRMPD spectral results.

Summarizing, IRMPD results indicate that all sodiated aliphatic AA complexes preferentially adopt a [N,CO] binding motif with some formation of the zwitterionic [CO_2^-] structures for Ala, Val, Leu, and Ile. These spectroscopic results are most consistent with predictions from the B3LYP and MP2 levels of theory. Although Na^+(hAla) was not evaluated in this spectroscopic study, the B3LYP and MP2 calculations indicate that it too should behave like its Ala and Val neighbors. Thus, in analyzing the TCID data below, thresholds were analyzed using both [N,CO]-tt_S(xx) and [CO_2^-]-cc(xx) as reactants, but with the former likely to dominate the results, as detailed below. In all cases, the neutral AA product formed upon dissociation is assumed to be the ttt(xx) conformer, found to be the ground structure in all the experimental studies of isolated AA, as detailed above.

Threshold Analysis

Threshold regions of the zero-pressure extrapolated cross sections for reaction 2 were analyzed using eq 1 as modified to include RRKM kinetics for dissociation. The analysis assumes that the transition states for dissociation are in the phase space limit (PSL) such that GS complexes dissociate to form GS neutral ligands. Given the length of time available for the complexes to dissociate, we believe this to be a reasonable assumption as the dissociating complex should be able to fully explore phase space, thereby allowing the neutral ligand to reach its GS conformation upon dissociation. Models that used Na^+(AA)[N,CO]-tt_S(xx) reactants and AA-ttt(xx) neutral products are shown in Figure 1 and can be seen to reproduce the experimental data well up to 4 – 5 eV and the entire cross section magnitudes. Such fits indicate that this model is appropriate for these systems and should lead to reliable thermochemistry. Table 3 gives values obtained for thresholds, E_0, and fitting parameters obtained from these analyses. Also given in Table 3 are the E_0 values obtained without use of RRKM, such that kinetic shifts for these processes can be determined. These kinetic shifts increase from 0.04 for the smallest system to 0.50 eV for the two

largest. These variations are a result of the gradually increasing BDE and the number of vibrational degrees of freedom as the side chain increases in size.

Analysis of the Na^+(Gly) system was unambiguous because all levels of theory indicated that only one GS was predicted for the sodiated complex and neutral AA product, Na^+(Gly)[N,CO]-tt and Gly-ttt, respectively. In contrast, in the remaining systems, different levels of theory predicted different GSs for the neutral AA product; however, in all cases, spectroscopic data detailed above indicate that the AA-ttt(xx) conformer is the GS, in agreement with most levels of theory. Therefore, all data was analyzed assuming this conformer was produced at threshold.

Likewise, several of the sodiated complexes were predicted to have different GS isomers at different levels of theory. In these cases, the complementary IRMPD data demonstrated that the [N,CO]-tt(xx) isomers are dominant. For AA = Ala, hAla, Val, Leu, and Ile, the IRMPD data also suggested the presence of [CO_2^-]-cc(xx) isomers. Therefore, thresholds were also determined using these alternative GSs, Table 3. In all cases, the thresholds shift by little, 0.01 eV for Ala, hAla, and Val, and slightly more significantly for Leu (0.03 eV) and Ile (0.05 eV). In all cases, the shifts remain well within the uncertainties. Nevertheless, as discussed further below, the threshold energies obtained by assuming a [CO_2^-]-cc(xx) reactant decrease from Val to Leu to Ile, whereas they increase when the [N,CO]-tt(xx) reactant is assumed. The latter trend agrees with literature results detailed below and is believed to be our most accurate interpretation of the data.

Also given in Table 3 are $\Delta S^{\ddagger}_{1000}$ values, which represent the degree of looseness for each of these reactions, where the PSL TS is assumed to lie at the centrifugal barrier for the association of Na^+ + AA. Consistent with PSL reactions, each of these values is positive. Furthermore, these $\Delta S^{\ddagger}_{1000}$ values generally increase as the size of the side chain increases: 47.9 (Gly), 50.0 (Ala), 50.5 (hAla), 51.6 (Val), 54.6 (Leu), and 55.7 (Ile) J/K mol.

Conversion of Thermodynamic Parameters from 0 K to 298 K

For comparison of the thermodynamic information obtained experimentally to room temperature conditions, Table 4 provides the conversion from 0 K thresholds to 298 K enthalpies

and Gibbs energies. This conversion is accomplished using the rigid rotor/harmonic oscillator approximation with rotational constants and vibrational frequencies calculated at the B3LYP/6-311+G(d,p) level for the [N,CO]-tt(xx) reactants and ttt(xx) products. Uncertainties listed are determined by scaling the vibrational frequencies by ± 10%. The accuracy of these conversions may be limited by inaccuracies in the low frequency vibrational modes. In particular, all these amino acids but glycine have methyl groups on their side chains, which may be more appropriately described as hindered rotors.

Discussion

Theoretical Results for Na^+–L Bond Dissociation Energies

Calculated BDEs for the Na^+(AA) systems of interest were determined at the B3LYP, B3P86, MP2, B3LYP-GD3BJ, and M06-2X levels of theory, as shown in Table 5. Given the assumption that species have sufficient time to adopt the GS conformation, these BDEs were calculated using energies for the complex GS at each level of theory, the AA neutral GS, and the Na^+ ion via equation 3,

$$D_0(Na^+–AA) = E_{AA} + E_{Na+} – E_{complex} \quad (3)$$

Generally, calculated BDEs increase as the size of the side chain increases such that average BDEs for Na^+(Gly), Na^+(Ala), Na^+(hAla), Na^+(Val), Na^+(Leu), Na^+(Ile) were determined to be 166.7 ± 6.5, 173.1 ± 7.4, 176.5 ± 8.1, 178.9 ± 8.3, 179.4 ± 7.5, and 181.1 ± 8.3 kJ/mol at all levels of theory (no BSSE corrections). The only exceptions were for B3LYP-GD3BJ and M06-2X, which predict that Na^+(Leu) is more weakly bound than Na^+(Val). Across all systems, MP2 predicts the lowest BDEs, whereas B3LYP-GD3BJ consistently suggests the highest BDEs (19 ± 2 kJ/mol higher in energy than MP2). The largest BSSE values were found at the MP2(full) level of theory, generally ~10 kJ/mol, whereas BSSEs at the remaining levels were ~3 kJ/mol.

Experiment versus Theory

The experimental and theoretical Na^+(AA) BDEs evaluated here are compared in Table 5.

Overall, theoretical predictions generally agree well with the experimental values lying within the experimental uncertainty except for MP2 values with BSSE corrections, M06-2X without BSSE corrections, and the B3LYP-GD3BJ values. For each level of theory, mean absolute deviations (MADs) from the TCID results were calculated in order to quantify the comparisons. For values with no BSSE corrections, MADs of 5 ± 2, 1 ± 1, 2 ± 1, 17 ± 3, and 9 ± 2 kJ/mol were calculated for the B3LYP, B3P86, MP2, B3LYP-GD3BJ, and M06-2X levels of theory, respectively. The MP2 level exhibits the smallest deviation from the experimental values, whereas B3LYP-GD3BJ is characterized by the largest deviations. Accounting for BSSE corrections results in MADs of 2 ± 1, 3 ± 1, 11 ± 1, 14 ± 3, and 7 ± 3 kJ/mol, respectively. (For B3LYP and B3P86 calculations, if the [N,CO] structures are used to calculate the BDEs for all complexes instead of the GS found at those levels, the MADs decrease by 1 kJ/mol for B3LYP and increase by 1 kJ/mol for B3P86 with and without BSSE.) Clearly, deviations at the MP2 level are significantly larger here such that BSSEs are systematically overestimated at this level of theory. Such large BSSE errors have been determined previously in similar systems.[14,96-98] Overall, the B3LYP-GD3BJ and M06-2X levels systematically overestimate the experimental BDEs, whereas B3LYP (with BSSE), B3P86 (with BSSE), and MP2 (without BSSE) provide very accurate reproduction of the TCID threshold energies measured here (within ~2 kJ/mol).

Comparison to Literature Values

Previous studies have evaluated the sodium ion affinities of the aliphatic amino acids via several experimental approaches.[11-16] Previous CID results are available for only AA = Gly from early work by Klassen et al.[12] and Moision and Armentrout.[14] The results of Klassen et al. correspond to a 0 K value of 151 ± 10 kJ/mol,[12] whereas our previous TCID result for Na^+(Gly) gave a dissociation energy at 0 K of 164 ± 6 kJ/mol,[14] which is clearly consistent with the threshold reported in the current work, 164 ± 7 kJ/mol. The discrepancy between the value of Klassen et al. and the latter TCID values have been discussed thoroughly in the previous study,[14] where the failure to account for the pressure dependence by Klassen et al. probably accounts for half the

discrepancy, with the remaining difference associated with the quadrupolar field in the collision region (rather than our octopolar field), which then led to different choices regarding the range of data analyzed. Importantly, the Na^+(Gly) complex in our previous work was generated using a DC discharge/flow tube source in which glycine was introduced into a meter long flow tube and formed the desired complex by 3-body collisional association. This source has been documented to yield ions that are thermalized by the $>10^5$ collisions with the flow gases (10% Ar in He).[99-104] Thus, the present study provides another example that the ESI source yields properly thermalized ions.

More complete results for the aliphatic acids have been obtained utilizing other experimental methods. The earliest results for AA = Gly, Ala, hAla, and Val were obtained using the kinetic method (KM) by Bojesen et al.[11] These authors were unable to find a suitable Na^+ reference base to anchor their values, so instead they anchored their scale to Na^+(Ala) obtained by setting its value to 75% of their value for Li^+(Ala). Nevertheless, the mean absolute deviations (MADs) between the results of Bojesen et al. and those from the present study are 5 ± 3 kJ/mol. If these values are reanchored by adjusting upward by 5 kJ/mol such that only relative values are considered, the MAD drops to 2 ± 2 kJ/mol. Thus, the progression of values in the two studies are in good agreement, as shown directly in Figure 5.

Later, Wesdemiotis and co-workers used KM to examine sodiated complexes of Gly, Ala, Val, Leu, and Ile, anchoring their results to a presumed 298 K value for Na^+(Ala) of 167.8 ± 8 kJ/mol determined relative to sodiated acetamide, N-methyl acetamide, and N,N-dimethyl acetamide values taken from theory.[16] (Notably, the theoretical values used for these three references are systematically higher than those determined using CID by Klassen et al. by 10 – 16 kJ/mol,[12] a discrepancy consistent with the discussion above for Gly.) Although the true temperature of these results is not known, their presumed 298 K relative values have been adjusted to 0 K using the thermochemistry calculated here and listed in Table 4. These values exhibit a MAD from the present work of 3 ± 2 kJ/mol, but an upwards adjustment of 3 kJ/mol brings the relative values within 1 ± 1 kJ/mol, indicating very similar trends, Figure 5.

The only other values available in the literature come from ligand-exchange equilibrium (Eq) studies of Gapeev and Dunbar. These authors originally studied the equilibrium of Ala with pyridine, obtaining a BDE for Na^+(Ala) of 159 ± 8 kJ/mol,[13] well below the other values in Table 5. They later examined a number of amino acids, including Gly, Ala, and Val,[15] anchoring their scale to that of Wesdemiotis and co-workers.[16] These values are shown in Table 5 and have a MAD from the present results of 3 ± 3 kJ/mol, which decreases to 2 ± 2 after reanchoring their scale by an upwards adjustment of 2 kJ/mol, Figure 5.

Although Figure 5 shows similar trends among all the data sets, it is worth commenting on the relative values of Gly and Ala, which differ by 3.1 kJ/mol in the present data set, 5.7 and 6.1 kJ/mol from the KM results,[11,16] and 8.1 kJ/mol from ligand exchange equilibria.[15] Although the values are within the experimental uncertainties in all cases, one imagines that the relative values should have better precision because many equivalent sources of error cancel. In addition, theoretical values range from 5.0 – 7.5 kJ/mol, in better agreement with the literature differences. Therefore, we considered whether the methyl rotor in Ala (and by extension all the heavier aliphatic AAs) needed to be treated as a hindered or free rotor. Calculations indicate that the vibrational frequency of this rotor changes little from the Na^+(Ala)[N,CO]-tt complex (220 cm^{-1}) to isolated AA-ttt (228 cm^{-1}), therefore, the methyl torsion was treated uniformly in both the reactant and neutral product. However, treating both as a free rotor led to a threshold shift of only +0.005 eV, which would change the relative TCID sodium cation affinities of Gly and Ala to 3.6 kJ/mol. Treatment as a hindered rotor would result in an even smaller change.

As pointed out by Hoyau and Ohanessian[64] and later by Rožman,[94] for the KM to acquire accurate thermodynamic information on the true ground structure of alkalated amino acids, the $(AA_1)Na^+(AA_2)$ heterodimer used to acquire the relative information should have the same binding mode as the $Na^+(AA_1)$ and $Na^+(AA_2)$ products. In particular, this is needed because the dissociation is typically performed at energies exceeding the threshold for fragmentation, hence there is little time available for reorganization. In contrast, equilibrium measurements allow sufficient time for species to rearrange upon dissociation, and TCID experiments bypass the use

of the heterodimer completely. Rožman calculated the relative energies of different structures of the sodiated heterodimers of Ile and its methyl ester, which forces the [N,CO]-ttt(xx) binding motif.[94] He found that the zwitterionic cc(g_t) binding was greatly disfavored in the heterodimer compared to the charge-solvated tt(g_t) binding motif, concluding that the KM could yield an excited isomer of the Na^+(AA) product. For the systems involved in the present study, this could lead to small changes in the relative energy differences in the final KM results.

Bond Dissociation Energy Trends

To explore the reasons for the incremental changes in BDEs for the sodiated aliphatic amino acids, we examined key structural aspects of the [N,CO] type ground structures. All systems exhibit Na^+–O distances of 2.23 – 2.24 Å (Figures 3 and 4), and likewise, ∠NNa^+O angles are quite similar, ranging from 72.2° – 73.0°. Some variations in Na^+–N distances are observed and decrease as the size of the amino acid increases: 2.47 Å for Gly, 2.45 Å for Ala, 2.44 Å for hAla, 2.43 Å for Val, 2.43 Å for Leu, and 2.42 Å for Ile. This observation suggests that the amino group becomes more electronegative with increasing side-chain length.

This latter effect can be quantified by examining how the experimental Na^+(AA) BDEs vary with polarizability of the amino acids (α). This trend is illustrated in Figure 6 and clearly shows that as the polarizability of the amino acid increases, the measured BDE increases linearly as BDE = 155.5 + 1.345 α (R^2 = 0.98). Here, polarizabilities, in $Å^3$, were taken from experimental results in solution,[105] except that for hAla, which is taken as the average of Ala and Val. (A very similar plot is obtained using isotropic polarizabilities calculated at the B3LYP/6-311+G(d,p) level, which yields values that are 94 ± 1 % of the solution phase polarizabilities. Here, the correlation is BDE = 155.3 + 1.445 α (R^2 = 0.98).) The linearity of this trend is also observed theoretically and using the other data listed in Table 5. It is perhaps notable that the present data provides the best correlation with polarizability among all these data sets.

Conclusion

Bond dissociation energies of Na^+(AA), where AA = glycine (Gly), alanine (Ala),

homoalanine (hAla), valine (Val), leucine (Leu), and isoleucine (Ile) were measured via kinetic energy dependent threshold collision-induced dissociation studies with Xe carried out in a guided ion beam tandem mass spectrometer. For all systems, loss of the intact neutral ligand from the complex is the only product channel observed. Experimental Na^+(AA) BDEs at 0 K adopt the following trend: Na^+(Gly) < Na^+(Ala) < Na^+(hAla) < Na^+(Val) < Na^+(Leu) < Na^+(Ile), in agreement with literature values and quantum chemical calculations. This trend can be explained by the increased polarizability of the aliphatic side chain. In particular, theoretical results at B3LYP, B3P86, and MP2(full)/6-311+G(2d,2p) level agree well with the experimental values, whereas B3LYP-GD3BJ and M06-2X predict BDEs larger than the experimental determinations. Likewise, the B3LYP and MP2 results agree with observations from IRMPD spectroscopic investigations of the same complexes (excluding hAla), whereas the other three levels of theory provide predictions that differ from these experimental results. Finally, spectroscopic results from the literature for the neutral AAs are best reproduced by B3LYP and MP2 calculations. Overall, these results indicate that all Na^+(AA) systems adopt [N,CO] GS conformations under experimental conditions, although for most systems, low-lying zwitterionic [CO_2^-] species were also located.

ASSOCIATED CONTENT

Supporting Information

Figures S1 – S10 show the pressure dependence of a representative Na^+(Ile) system; low-energy conformers of Gly, Ala, hAla, Val, Leu, and Ile; and select higher energy structures located for Na^+(Gly), Na^+(Ala), Na^+(hAla), Na^+(Val), Na^+(Leu), and Na^+(Ile). Tables S1 – S9 give theoretical relative energies for higher energy species of Gly, Ala, hAla, Val, Leu, Ile, Na^+(Gly), Na^+(Ala), Na^+(hAla), Na^+(Val), Na^+(Leu), and Na^+(Ile) species.

AUTHOR INFORMATION

Corresponding Author

P. B. Armentrout - Department of Chemistry, University of Utah, 315 S. 1400 E. Rm. 2020, Salt Lake City, Utah 84112, United States; orcid.org/0000-0003-2953-6039;

Email: armentrout@chem.utah.edu

Authors

Hanh D. M. Pham, Georgia C. Boles - Department of Chemistry, University of Utah, 315 S. 1400 E. Rm. 2020, Salt Lake City, Utah 84112, United States

ACKNOWLEDGMENTS

The authors acknowledge support for this work by the National Science Foundation, Grant CHE-1954142. The authors also gratefully acknowledge a grant of computer time from the Center for High Performance Computing at the University of Utah.

REFERENCES

(1) Ibers, J. A.; Holm, R. H. Modeling Coordination Sites in Metallobiomolecules. *Science* **1980,** *209*, 223-235.

(2) Jorgensen, P. L.; Hakansson, K. O.; Karlish, S. J. Structure and mechanism of Na,K-ATPase: functional sites and their interactions. *Annu. Rev. Physiol.* **2003,** *65*, 817-849.

(3) Page, M. J.; Macgillivray, R. T.; Di Cera, E. Determinants of specificity in coagulation proteases. *J. Thromb. Haemost.* **2005,** *3*, 2401-2408.

(4) Page, M. J.; Di Cera, E. Role of Na^+ and K^+ in enzyme function. *Physiol. Rev.* **2006,** *86*, 1049-1092.

(5) Furutani, Y.; Murata, T.; Kandori, H. Sodium or Lithium Ion-Binding-Induced Structural Changes in the K-Ring of V-ATPase from Enterococcus hirae Revealed by ATR-FTIR Spectroscopy. *J. Am. Chem. Soc* **2011,** *133*, 2860-2863.

(6) Banerjee, U.; Dasgupta, A.; Rout, J. K.; Singh, O. P. Effects of lithium therapy on Na^+–K^+-ATPase activity and lipid peroxidation in bipolar disorder. *Prog. Neuropsychopharmacol Biol. Psychiatry* **2012,** *37*, 56-61.

(7) Hodgkin, A. L.; Huxley, A. F. A quantitative description of membrane current and its application to conduction and excitation in nerve. *J. Physiology* **1952,** *117*, 500-544.

(8) Glitsch, H. G. Electrophysiology of the sodium-potassium-ATPase in cardiac cells. *Physiol. Rev.* **2001,** *81*, 1791-1826.

(9) Forrest, M. D. The sodium-potassium pump is an information processing element in brain computation. *Front Physiol* **2014,** *5*, 472-472.

(10) Andersen, L. J.; Norsk, P.; Johansen, L. B.; Christensen, P.; Engstrøm, T.; Bie, P. Osmoregulatory control of renal sodium excretion after sodium loading in humans. *Am. J.*

Physiology-Regulatory, Integrative and Comparative Physiology **1998,** *275*, R1833-R1842.

(11) Bojesen, G.; Breindahl, T.; Andersen, U. N. On the Sodium and Lithium Ion Affinities of Some α-Amino Acids. *Org. Mass Spectrom.* **1993,** *28*, 1448-1452.

(12) Klassen, J. S.; Anderson, S. G.; Blades, A. T.; Kebarle, P. Reaction Enthalpies for $M^+L = M^+ + L$, Where $M^+ = Na^+$ and K^+ and L = Acetamide, N-methylacetamide, N,N-dimethylacetamide, Glycine, and Glycylglycine, from Determinations of the Collision-induced Dissociation Thresholds. *J. Phys. Chem.* **1996,** *100*, 14218-14227.

(13) Gapeev, A.; Dunbar, R. C. Cation-Pi Interactions and the Gas-Phase Thermochemistry of the Na^+/Phenylalanine Complex. *J. Am. Chem. Soc.* **2001,** *123*, 8360-8365.

(14) Moision, R. M.; Armentrout, P. B. An Experimental and Theoretical Dissection of Sodium Cation/Glycine Interactions. *J. Phys. Chem. A* **2002,** *106*, 10350-10362.

(15) Gapeev, A.; Dunbar, R. C. Na^+ Affinities of Gas-phase Amino Acids by Ligand Exchange Equilibrium. *Int. J. Mass Spectrom.* **2003,** *228*, 825-839.

(16) Kish, M. M.; Ohanessian, G.; Wesdemiotis, C. The Na^+ Affinities of α-Amino Acids: Side-chain Substituent Effects. *Int. J. Mass Spectrom.* **2003,** *227*, 509-524.

(17) Ruan, C.; Rodgers, M. T. Cation-π Interactions: Structures and Energetics of Complexation of Na^+ and K^+ with the Aromatic Amino Acids, Phenylalanine, Tyrosine and Tryptophan. *J. Am. Chem. Soc.* **2004,** *126*, 14600-14610.

(18) Moision, R. M.; Armentrout, P. B. The Special Five-membered Ring of Proline: An Experimental and Theoretical Investigation of Alkali Metal Cation Interactions with Proline and Its Four- and Six-membered Ring Analogues. *J. Phys. Chem. A* **2006,** *110*, 3933-3946.

(19) Heaton, A. L.; Armentrout, P. B. Thermodynamics and Mechanism of the Deamidation of Sodium-Bound Asparagine. *J. Am. Chem. Soc.* **2008,** *130*, 10227-10232.

(20) Heaton, A. L.; Moision, R. M.; Armentrout, P. B. Experimental and Theoretical Studies of Sodium Cation Interactions with the Acidic Amino Acids and Their Amide Derivatives. *J. Phys. Chem. A* **2008,** *112*, 3319-3327.

(21) Ye, S. J.; Clark, A. A.; Armentrout, P. B. An Experimental and Theoretical Investigation of Alkali Metal Cation Interactions with Hydroxyl Side Chain Amino Acids. *J. Phys. Chem. B* **2008,** *112*, 10291-10302.

(22) Wang, P.; Ohanessian, G.; Wesdemiotis, C. The Sodium Ion Affinities of Asparagine, Glutamine, Histidine and Arginine. *Int. J. Mass Spectrom.* **2008,** *269*, 34-45.

(23) Armentrout, P. B.; Gabriel, A.; Moision, R. M. An Experimental and Theoretical Study of Alkali Metal Cation/Methionine Interactions. *Int. J. Mass Spectrom.* **2009,** *283*, 56-68.

(24) Armentrout, P. B.; Armentrout, E. I.; Clark, A. A.; Cooper, T. E.; Stennett, E. M. S.; Carl, D. R. An Experimental and Theoretical Study of Alkali Metal Cation Interactions with Cysteine. *J. Phys. Chem. B* **2010,** *114*, 3927-3937.

(25) Armentrout, P. B.; Citir, M.; Chen, Y.; Rodgers, M. T. Thermochemistry of Alkali Metal Cation Interactions with Histidine: Influence of the Side-Chain. *J. Phys. Chem. A* **2012,** *116*, 11823-11832.

(26) Ye, S. J.; Armentrout, P. B. An Experimental and Theoretical Investigation of the Decomposition of Lithiated Hydroxyl Side Chain Amino Acids. *J. Phys. Chem. B* **2008,** *112*, 10303-10313.

(27) Bowman, V. N.; Heaton, A. L.; Armentrout, P. B. Metal Cation Dependence of Interactions with Amino Acids: Bond Energies of Rb^+ to Gly, Ser, Thr, and Pro. *J. Phys. Chem. B* **2010,** *114*, 4107-4114.

(28) Tsang, Y.; Wong, C. C. L.; Wong, C. H. S.; Cheng, J. M. K.; Ma, N. L.; Tsang, C. W. Proton

and Potassium Affinities of Aliphatic and N-Methylated Aliphatic α-Amino Acids: Effect of Alkyl Chain Length on Relative Stabilities of K^+ Bound Zwitterionic Complexes. *Int. J. Mass Spectrom.* **2012,** *316-318*, 273-283.

(29) Armentrout, P. B.; Yang, B.; Rodgers, M. T. Metal Cation Dependence of Interactions with Amino Acids: Bond Energies of Rb^+ and Cs^+ to Met, Phe, Tyr, and Trp. *J. Phys. Chem. B* **2013,** *117*, 3771-3781.

(30) Armentrout, P. B.; Yang, B.; Rodgers, M. T. Metal Cation Dependence of Interactions with Amino Acids: Bond Dissociation Energies of Rb^+ and Cs^+ to the Acidic Amino Acids and Their Amide Derivatives. *J. Phys. Chem. B* **2014,** *118*, 4300–4314.

(31) Mookherjee, A.; Armentrout, P. B. Theoretical Investigation and Reinterpretation of the Decomposition of Lithiated Proline and N-Methyl Proline. *Int. J. Mass Spectrom.* **2014,** *370*, 16-28.

(32) Bourcier, S.; Chia, R. X.; Bimbong, R. N. B.; Bouchoux, G. Gas-phase lithium cation affinity of glycine. *Eur. J. Mass Spectrom.* **2015,** *21*, 149-159.

(33) Armentrout, P. B.; Boles, G. C.; Ghiassee, M.; Berden, G.; Oomens, J. Infrared Multiple Photon Dissociation Spectra of Sodiated Complexes of the Aliphatic Amino Acids. **2021**, submitted for publication.

(34) Ervin, K. M.; Armentrout, P. B. Translational Energy Dependence of $Ar^+ + XY \rightarrow ArX^+ + Y$ ($XY = H_2, D_2, HD$) from Thermal to 30 eV c.m. *J. Chem. Phys.* **1985,** *83*, 166-189.

(35) Muntean, F.; Armentrout, P. B. Guided Ion Beam Study of Collision-Induced Dissociation Dynamics: Integral and Differential Cross Sections. *J. Chem. Phys.* **2001,** *115*, 1213-1228.

(36) Armentrout, P. B. Not Just a Structural Tool: The Use of Guided Ion Beam Tandem Mass Spectrometry to Determine Thermochemistry. *J. Am. Soc. Mass Spectrom.* **2002,** *13*, 419-434.

(37) Moision, R. M.; Armentrout, P. B. An Electrospray Ionization Source for Thermochemical Investigation with the Guided Ion Beam Mass Spectrometer. *J. Am. Soc. Mass Spectrom.* **2007,** *18*, 1124-1134.

(38) Kim, T.; Tolmachev, A. V.; Harkewicz, R.; Prior, D. C.; Anderson, G.; Udseth, H. R.; Smith, R. D.; Bailey, T. H.; Rakov, S.; Futrell, J. H. Design and Implementation of a New Electrodynamic Ion Funnel. *Anal. Chem* **2000,** *72*, 2247-2255.

(39) Ye, S. J.; Armentrout, P. B. Absolute Thermodynamic Measurements of Alkali Metal Cation Interactions with a Simple Dipeptide and Tripeptide. *J. Phys. Chem. A* **2008,** *112*, 3587-3596.

(40) Heaton, A. L.; Armentrout, P. B. Thermodynamics and Mechanism of Protonated Asparagine Decomposition. *J. Am. Soc. Mass Spectrom.* **2009,** *20*, 852-866.

(41) Carpenter, J. E.; McNary, C. P.; Furin, A.; Sweeney, A. F.; Armentrout, P. B. How Hot are Your Ions Really? A Threshold Collision-Induced Dissociation Study of Substituted Benzylpyridinium "Thermometer" Ions. *J. Am. Soc. Mass Spectrom.* **2017,** *28*, 1876-1888.

(42) Teloy, E.; Gerlich, D. Integral Cross Sections for Ion-Molecule Reactions. 1. The Guided Beam Technique. *Chem. Phys.* **1974,** *4*, 417-427.

(43) Gerlich, D., Inhomogeneous rf Fields: A Versatile Tool for the Study of Processes with Slow Ions. In *Adv. Chem. Phys.*, Ng, C.-Y.; Baer, M., Eds. Wiley: 1992; Vol. 82, pp 1-176.

(44) Aristov, N.; Armentrout, P. B. Collision-Induced Dissociation of Vanadium Monoxide Ion. *J. Phys. Chem.* **1986,** *90*, 5135-5140.

(45) Dalleska, N. F.; Honma, K.; Sunderlin, L. S.; Armentrout, P. B. Solvation of Transition Metal Ions by Water. Sequential Binding Energies of $M^+(H_2O)_x$ (x = 1 - 4) for M = Ti - Cu Determined by Collision-Induced Dissociation. *J. Am. Chem. Soc.* **1994,** *116*, 3519-3528.

(46) Daly, N. R. Scintillation Type Mass Spectrometer Ion Detector. *Rev. Sci. Instrum.* **1960,** *31*,

264-267.
(47) Beyer, T. S.; Swinehart, D. F. Number of Multiply-Restricted Partitions. *Commun. ACM* **1973,** *16*, 379.
(48) Stein, S. E.; Rabinovich, B. S. On the Use of Exact State Counting Methods in RRKM Rate Calculations. *Chem. Phys. Lett.* **1977,** *49*, 183-188.
(49) Stein, S. E.; Rabinovitch, B. S. Accurate Evaluation of Internal Energy Level Sums and Densities Including Anharmonic Oscillators and Hindered Rotors. *J. Chem. Phys.* **1973,** *58*, 2438-2445.
(50) Gilbert, R. G.; Smith, S. C. *Theory of Unimolecular and Recombination Reactions*. Blackwell Scientific: London, 1990.
(51) Armentrout, P. B.; Ervin, K. M.; Rodgers, M. T. Statistical Rate Theory and Kinetic Energy-Resolved Ion Chemistry – Theory and Applications. *J. Phys. Chem. A* **2008,** *112*, 10071-10085.
(52) Rodgers, M. T.; Ervin, K. M.; Armentrout, P. B. Statistical Modeling of Collision-Induced Dissociation Thresholds. *J. Chem. Phys.* **1997,** *106*, 4499-4508.
(53) Waage, E. V.; Rabinovitch, B. S. Centrifugal Effects in Reaction Rate Theory. *Chem. Rev.* **1970,** *70*, 377-387.
(54) Rodgers, M. T.; Armentrout, P. B. Absolute Binding Energies of Lithium Ions to Short Chain Alcohols, $C_nH_{n+2}O$, n = 1 - 4, Determined by Threshold Collision-Induced Dissociation. *J. Phys. Chem. A* **1997,** *101*, 2614-2625.
(55) More, M. B.; Ray, D.; Armentrout, P. B. Cation-Ether Complexes in the Gas Phase: Bond Dissociation Energies of Na^+(dimethyl ether)$_x$, x = 1 - 4; Na^+(1,2-dimethoxyethane)$_x$, x = 1 and 2; and Na^+(12-crown-4). *J. Phys. Chem. A* **1997,** *101*, 831-839.
(56) More, M. B.; Ray, D.; Armentrout, P. B. Cation-Ether Complexes in the Gas Phase: Bond Dissociation Energies of K^+(dimethyl ether)$_x$, x = 1 - 4; K^+(1,2-dimethoxyethane)$_x$, x = 1 and 2; and K^+(12-crown-4). *J. Phys. Chem. A* **1997,** *101*, 4254-4262.
(57) More, M. B.; Ray, D.; Armentrout, P. B. Cation-Ether Complexes in the Gas Phase: Bond Dissociation Energies of M^+(dimethyl ether)$_x$, x = 1 - 3, M^+(1,2-dimethoxyethane)$_x$, x = 1 and 2, and M^+(12-crown-4) Where M = Rb and Cs. *J. Phys. Chem. A* **1997,** *101*, 7007-7017.
(58) Armentrout, P. B.; Simons, J. Understanding Heterolytic Bond Cleavage. *J. Am. Chem. Soc.* **1992,** *114*, 8627-8633.
(59) Frisch, M. J.; Trucks, G. W.; Schlegel, H. B.; Scuseria, G. E.; Robb, M. A.; Cheeseman, J. R.; Scalmani, G.; Barone, V.; Mennucci, B.; Petersson, G. A., et al. *Gaussian 09, Revision D.01* Gaussian, Inc.: Wallingford, CT, USA, 2009.
(60) Becke, A. D. Density-functional Exchange Energy Approximation with Correct Asymptotic Behavior. *Phys. Rev. A* **1988,** *38*, 3098-3100.
(61) Lee, C.; Yang, W.; Parr, R. G. Development of the Colle-Salvetti Correlation-Energy Formula into a Functional of the Electron Density. *Phys. Rev. B* **1988,** *37*, 785-789.
(62) Ditchfield, R.; Hehre, W. J.; Pople, J. A. Self-Consistent Molecular-Orbital Methods. IX. An Extended Gaussian-Type Basis for Molecular-Orbital Studies of Organic Molecules. *J. Chem. Phys.* **1971,** *54*, 724-728.
(63) Jensen, F. Structure and Stability of Complexes of Glycine and Glycine Methyl Analogues with H^+, Li^+, and Na^+. *J. Am. Chem. Soc.* **1992,** *114*, 9533-9537.
(64) Hoyau, S.; Ohanessian, G. Interaction of Alkali Metal Cations (Li^+ - Cs^+) with Glycine in the Gas Phase: A theoretical Study. *Chem. Eur. J.* **1998,** *4*, 1561-1569.
(65) Marino, T.; Russo, N.; Toscano, M. Gas-phase metal ion (Li^+, Na^+, Cu^+) affinities of glycine and alanine. *J. Inorg. Biochem.* **2000,** *79*, 179-185.

(66) Foresman, J. B.; Frisch, A. E. *Exploring Chemistry with Electronic Structure Methods*. 2nd ed.; Gaussian, Inc.: Pittsburgh, PA, 1996.
(67) Möller, C.; Plesset, M. S. Note on an Approximation Treatment for Many-Electron Systems. *Phys. Rev.* **1934,** *46*, 618-622.
(68) Krishnan, R.; Binkley, J. S.; Seeger, R.; Pople, J. A. Self-consistent Molecular Orbital Methods. XX. A Basis Set for Correlated Wave Functions. *J. Chem. Phys.* **1980,** *72*, 650-654.
(69) Grimme, S.; Antony, J.; Ehrlich, S.; Krieg, H. A Consistent and Accurate Ab Initio Parametrization of Density Functional Dispersion Correction (DFT-D) for the 94 Elements H-Pu. *J. Chem. Phys.* **2010,** *132*, 154104-154119.
(70) Grimme, S.; Ehrlich, S.; Goerigk, L. Effect of the Damping Function in Dispersion Corrected Density Functional Theory. *J. Comput. Chem.* **2011,** *32*, 1456-1465.
(71) Zhao, Y.; Truhlar, D. G. The M06 Suite of Density Functionals for Main Group Thermochemistry, Thermochemical Kinetics, Noncovalent Interactions, Excited States, and Transition Elements: Two New Functionals and Systematic Testing of Four M06-Class Functionals and 12 Other Functionals. *Theor. Chem. Acc.* **2008,** *120*, 215-241.
(72) Boys, S. F.; Bernardi, R. The Calculation of Small Molecular Interactions by the Differences of Separate Total Energies. Some Procedures with Reduced Errors. *Mol. Phys.* **1970,** *19*, 553-566.
(73) Jensen, J. H.; Gordon, M. S. Conformational potential energy surface of glycine: a theoretical study. *J. Am. Chem. Soc.* **1991,** *113*, 7917-7924.
(74) Godfrey, P. D.; Brown, R. D. Shape of Glycine. *J. Am. Chem. Soc.* **1995,** *117*, 2019-2023.
(75) Conte, R.; Houston, P. L.; Qu, C.; Li, J.; Bowman, J. M. Full-dimensional, ab initio potential energy surface for glycine with characterization of stationary points and zero-point energy calculations by means of diffusion Monte Carlo and semiclassical dynamics. *J. Chem. Phys.* **2020,** *153*, 244301.
(76) Stepanian, S. G.; Reva, I. D.; Radchenko, E. D.; Rosado, M. T. S.; Duarte, M. L. T. S.; Fausto, R.; Adamowicz, L. Matrix-Isolation Infrared and Theoretical Studies of the Glycine Conformers. *J. Phys. Chem. A* **1998,** *102*, 1041-1054.
(77) Ivanov, A. Y.; Sheina, G.; Blagoi, Y. P. FTIR spectroscopic study of the UV-induced rotamerization of glycine in the low temperature matrices (Kr, Ar, Ne). *Spectrochim. Acta A: Molec. Biomolec. Spectros.* **1998,** *55*, 219-228.
(78) Gronert, S.; O'Hair, R. A. J. Ab Initio Studies of Amino Acid Conformations. 1. The Conformers of Alanine, Serine, and Cysteine *J. Am. Chem. Soc.* **1995,** *117*, 2071-2081.
(79) Blanco, S.; Lesarri, A.; López, J. C.; Alonso, J. L. The Gas-Phase Structure of Alanine. *J. Am. Chem. Soc.* **2004,** *126*, 11675-11683.
(80) Lee, G.-Y. A DFT Study of the Intramolecular Hydrogen Bonding of Alanine and Its Effects on Ionization Energies. *J. Kor. Chem. Soc.* **2015,** *59*, 541-544.
(81) Stepanian, S. G.; Reva, I. D.; Radchenko, E. D.; Adamowicz, L. Conformational Behavior of α-Alanine. Matrix-Isolation Infrared and Theoretical DFT and ab Initio Study. *J. Phys. Chem. A* **1998,** *102*, 4623-4629.
(82) Cocinero, E. J.; Lesarri, A.; Sanz, M. E.; López, J. C.; Alonso, J. L. Conformations of α-Aminobutyric Acid in the Gas Phase. *ChemPhysChem* **2006,** *7*, 1481-1487.
(83) Lesarri, A.; Cocinero, E. J.; López, J. C.; Alonso, J. L. The Shape of Neutral Valine. *Angew. Chem. Int. Ed.* **2004,** *43*, 605-610.
(84) Dokmaisrijan, S.; Lee, V. S.; Nimmanpipug, P. The gas phase conformers and vibrational spectra of valine, leucine and isoleucine: An ab initio study. *J. Molec. Structure: THEOCHEM* **2010,** *953*, 28-38.

(85) Stepanian, S. G.; Reva, I. D.; Radchenko, E. D.; Adamowicz, L. Combined Matrix-Isolation Infrared and Theoretical DFT and ab Initio Study of the Nonionized Valine Conformers. *J. Phys. Chem. A* **1999,** *103*, 4404-4412.

(86) Cocinero, E. J.; Lesarri, A.; Grabow, J.-U.; López, J. C.; Alonso, J. L. The Shape of Leucine in the Gas Phase. *ChemPhysChem* **2007,** *8*, 599-604.

(87) Stepanian, S. G.; Ivanov, A. Y.; Adamowicz, L. Conformational composition of neutral leucine. Matrix isolation infrared and ab initio study. *Chem. Phys.* **2013,** *423*, 20-29.

(88) Lesarri, A.; Sánchez, R.; Cocinero, E. J.; López, J. C.; Alonso, J. L. Coded Amino Acids in Gas Phase: The Shape of Isoleucine. *J. Am. Chem. Soc.* **2005,** *127*, 12952-12956.

(89) Boeckx, B.; Nelissen, W.; Maes, G. Potential energy surface and matrix isolation FT-IR study of isoleucine. *J. Phys. Chem. A* **2012,** *116*, 3247-58.

(90) Wyttenbach, T.; Witt, M.; Bowers, M. T. On the Stability of Amino Acid Zwitterions in the Gas Phase: The Influence of Derivatization, Proton Affinity, and Alkali Ion Addition. *J. Am. Chem. Soc.* **2000,** *122*, 3458-3464.

(91) Bouchonnet, S.; Hoppilliard, Y. Proton and Sodium Ion Affinities of Glycine and Its Sodium Salt in the Gas Phase. Ab Initio Calculations. *Org. Mass Spectrom.* **1992,** *27*, 71-76.

(92) Marino, T.; Russo, N.; Toscano, M. Potential Energy Surfaces for the Gas-Phase Interaction between α-Alanine and Alkali Metal Ions (Li^+, Na^+, K^+). A Density Functional Study. *Inorg. Chem.* **2001,** *40*, 6439-6443.

(93) Lemoff, A. S.; Bush, M. F.; Williams, E. R. Binding energies of water to sodiated valine and structural isomers in the gas phase: The effect of proton affinity on zwitterion stability. *J. Am. Chem. Soc.* **2003,** *125*, 13576–13584.

(94) Rožman, M. Theoretical study of the gas-phase structures of sodiated and cesiated leucine and isoleucine: zwitterionic structure disfavored in kinetic method experiments. *J. Mass Spectrom.* **2005,** *40*, 1357-1361.

(95) Kapota, C.; Lemaire, J.; Maitre, P.; Ohanessian, G. Vibrational Signature of Charge Solvation vs Salt Bridge Isomers of Sodiated Amino Acids in the Gas Phase. *J. Am. Chem. Soc.* **2004,** *126*, 1836-1842.

(96) Feller, D. A Complete Basis Set Estimate of Cation-bond Strengths: Na^+(ethylene) and Na^+(benzene). *Chem. Phys. Lett.* **2000,** *322*, 543-548.

(97) Chinthaka, S. D. M.; Chu, Y.; Rannulu, N. S.; Rodgers, M. T. Sodium Cation Affinities of MALDI Matrices Determined by Guided Ion Beam Tandem Mass Spectrometry: Application to Benzoic acid Derivatives *J. Phys. Chem. A* **2006,** *110*, 1426-1437.

(98) Chinthaka, S. D. M.; Rodgers, M. T. Sodium Cation Affinities of Commonly Used MALDI Matrices Determined by Guided Ion Beam Tandem Mass Spectrometry *J. Am. Soc. Mass Spectrom.* **2012,** *23*, 676-689.

(99) Schultz, R. H.; Crellin, K. C.; Armentrout, P. B. Sequential Bond Energies of $Fe(CO)_x^+$ (x = 1 - 5): Systematic Effects on Collision-Induced Dissociation Measurements. *J. Am. Chem. Soc.* **1991,** *113*, 8590-8601.

(100) Schultz, R. H.; Armentrout, P. B. A Guided-Ion Beam Study of the Reactions of N_4^+ with H_2, HD, and D_2: An Evaluation of Psuedo-Arrhenius Analyses of Ion-Molecule Reaction Systems. *J. Chem. Phys.* **1992,** *96*, 1046-1052.

(101) Fisher, E. R.; Kickel, B. L.; Armentrout, P. B. Collision-Induced Dissociation and Charge Transfer Reactions of SiF_x^+ (x = 1 - 4).Thermochemistry of SiF_x and SiF_x^+. *J. Phys. Chem.* **1993,** *97*, 10204-10210.

(102) Khan, F. A.; Clemmer, D. E.; Schultz, R. H.; Armentrout, P. B. Sequential Bond Energies

of $Cr(CO)_x^+$, x = 1 - 6. *J. Phys. Chem.* **1993,** *97*, 7978-7987.

(103) Dalleska, N. F.; Honma, K.; Armentrout, P. B. Stepwise Solvation Enthalpies of Protonated Water Clusters: Collision Induced Dissociation as an Alternative to Equilibrium Studies. *J. Am. Chem. Soc.* **1993,** *115*, 12125-12131.

(104) Dalleska, N. F.; Tjelta, B. L.; Armentrout, P. B. Sequential Bond Energies of Water to Na^+ ($3s^0$), Mg^+($3s^1$), and Al^+ ($3s^2$). *J. Phys. Chem* **1994,** *98*, 4191-4195.

(105) McMeekin, T. L.; Wilensky, M.; Groves, M. L. Refractive indices of proteins in relation to amino acid composition and specific volume. *Biochem. Biophys. Res. Commun.* **1962,** *7*, 151-156.

Table 1. Relative 0 K Enthalpies (298 K Gibbs Energies) (kJ/mol) of Gly, Ala, hAla, Val, Leu, and Ile Low-Energy Conformers Calculated at Several Levels of Theory [a]

AA	Conformer	B3LYP[b]	B3P86[b]	MP2(full)[b]	B3LYP-GD3BJ[c]	M06-2X[c]
Gly	ttt	**0.0 (0.0)**	**0.0 (0.0)**	**0.0 (0.0)**	**0.0 (0.0)**	**0.0 (0.0)**
	ccc	3.7 (4.5)	1.1 (1.8)	3.6 (4.3)	3.1 (3.9)	6.2 (7.2)
	ttg	5.3 (6.1)	5.1 (5.9)	4.7 (5.5)	5.4 (6.3)	5.5 (6.4)
	tct	6.7 (3.8)	6.7 (3.8)	6.9 (3.9)	6.8 (4.2)	7.3 (4.4)
Ala	ttt	**0.0 (0.0)**	1.1 (**0.0**)	**0.0 (0.0)**	**0.0 (0.0)**	**0.0 (0.0)**
	ccc_S	1.9 (3.1)	**0.0** (0.1)	2.0 (3.2)	0.9 (2.2)	3.7 (5.2)
	ccc_A	2.2 (3.5)	0.0_3 (0.3)	3.3 (4.7)	1.3 (2.7)	4.1 (5.5)
	ttg_-	4.9 (5.5)	5.9 (5.4)	4.5 (5.1)	4.8 (5.5)	5.2 (6.1)
hAla	ttt(t)	**0.0 (0.0)**	1.4 (**0.0**)	**0.0 (0.0)**	**0.0 (0.0)**	**0.0 (0.0)**
	ccc(t)	1.9 (3.4)	**0.0** (0.0_4)	3.2 (4.6)	0.6 (1.9)	3.0 (4.1)
	ttt(g_-)	2.7 (2.7)	3.9 (2.6)	0.5 (0.6)	0.7 (0.9)	0.2 (1.1)
	ttt(g_+)	3.2 (3.0)	5.1 (3.5)	2.2 (2.1)	2.1 (2.1)	3.0 (3.9)
Val	ttt(c)	**0.0 (0.0)**	2.4 (0.8)	**0.0 (0.0)**	1.1 (**0.0**)	**0.0 (0.0)**
	ccc(c_+)	0.9 (2.5)	**0.0 (0.0)**	2.3 (3.9)	**0.0** (0.8)	2.8 (3.7)
	ttt(g_-)	2.0 (2.1)	4.8 (3.4)	2.5 (2.6)	2.9 (2.5)	3.3 (3.8)
	tgt(g_-)	4.1 (4.1)	7.2 (5.7)	4.1 (4.1)	5.0 (4.4)	5.8 (5.9)
Leu	ttt(tg_+)	**0.0 (0.0)**	0.8 (**0.0**)	**0.0 (0.0)**	**0.0 (0.0)**	**0.0 (0.0)**
	ccc(tg_+)	2.6 (4.7)	**0.0** (1.3)	3.9 (6.1)	2.2 (2.2)	4.7 (5.5)
	ttt(g_+g_-)	4.0 (5.8)	5.3 (6.3)	1.9 (3.7)	2.7 (2.7)	3.1 (4.4)
	ccc(g_+g_-)	4.8 (7.0)	2.7 (4.1)	2.6 (4.8)	4.3 (4.3)	4.6 (7.1)
Ile	ttt(g_-t)	**0.0 (0.0)**	2.8 (0.7)	**0.0 (0.0)**	1.1 (**0.0**)	**0.0 (0.0)**
	ccc(g_-t)	0.4 (2.5)	**0.0 (0.0)**	1.4 (3.5)	**0.0** (0.9)	3.4 (5.6)
	tgt(tt)	1.8 (2.9)	5.0 (4.0)	2.7 (3.8)	3.4 (3.0)	4.0 (5.4)
	tg_-t(tt)	3.9 (4.6)	7.4 (6.0)	4.1 (4.8)	5.6 (5.2)	6.3 (6.8)

[a] Ground structure in bold. [b] Calculations performed at the stated level of theory using a 6-311+G(2d,2p) basis set with geometries calculated at the B3LYP/6-311+G(d,p) level.

[c] Calculations performed at the stated level of theory using a 6-311+G(2d,2p) basis set with geometries and zero-point energies calculated using a 6-311+G(d,p) basis set.

Table 2. Relative 0 K Enthalpies (298 K Gibbs Energies) (kJ/mol) of Na^+(AA) Low-Energy Species Calculated at Several Levels of Theory [a]

AA	Conformer	B3LYP[b]	B3P86[b]	MP2(full) [b]	B3LYP-GD3BJ[c]	M06-2X[c]
Gly	[N,CO]-tt	**0.0 (0.0)**	**0.0 (0.0)**	**0.0 (0.0)**	**0.0 (0.0)**	**0.0 (0.0)**
	[CO]-cc	10.4 (7.2)	6.2 (3.0)	11.8 (8.7)	13.8 (10.4)	15.3 (10.8)
	[CO_2^-]-cc	10.5 (10.7)	7.4 (7.6)	7.6 (7.8)	13.5 (13.6)	19.4 (19.1)
	[CO,OH]-cc	10.7 (9.3)	6.5 (5.2)	9.1 (7.8)	13.7 (12.2)	13.5 (12.4)
Ala	[N,CO]-tt_S	**0.0 (0.0)**	**0.0 (0.0)**	**0.0 (0.0)**	**0.0 (0.0)**	**0.0 (0.0)**
	[N,CO]-tt_A	1.8 (1.4)	1.5 (1.1)	3.0 (2.6)	2.6 (1.9)	2.2 (1.9)
	[CO_2^-]-cc	3.7 (3.2)	0.7 (0.2)	3.9 (3.4)	8.1 (7.2)	14.2 (13.1)
	[CO,OH]-cc	9.6 (7.7)	5.3 (3.4)	9.7 (7.8)	13.9 (11.8)	13.7 (11.3)
hAla	[N,CO]-tt_S(t)	**0.0 (0.0)**	1.3 (1.8)	0.3 (0.1)	1.5 (0.8)	1.9 (0.9)
	[CO_2^-]-cc(t)	1.5 (1.1)	**0.0 (0.0)**	2.3 (1.7)	7.7 (6.2)	13.7 (12.6)
	[N,CO]-tt_A(t)	2.2 (2.0)	3.2 (3.5)	3.5 (3.2)	4.3 (3.1)	3.0 (2.6)
	[N,CO]-$tt_S(g_-)$	2.3 (2.5)	3.2 (3.9)	**0.0 (0.0)**	**0.0 (0.0)**	**0.0 (0.0)**
	[N,CO]-$tt_S(g_+)$	2.7 (2.9)	4.2 (4.9)	1.8 (1.8)	3.4 (3.0)	3.5 (3.3)
	[N,CO]-$tt_A(g_-)$	3.0 (3.1)	3.8 (4.4)	2.3 (2.3)	3.5 (2.4)	2.7 (2.6)
	[CO_2^-]-cc(g_-)	3.6 (3.2)	1.8 (1.8)	2.1 (1.6)	7.9 (6.7)	13.8 (12.3)
Val	[CO_2^-]-cc(g_+)	**0.0 (0.0)**	**0.0 (0.0)**	0.7 (0.5)	6.5 (5.9)	11.4 (10.0)
	[N,CO]-$tt_S(g_+)$	0.7 (0.9)	3.1 (3.3)	**0.0 (0.0)**	**0.0 (0.0)**	**0.0 (0.0)**
	[N,CO]-$tt_A(g_+)$	1.3 (1.4)	3.7 (4.0)	3.5 (2.4)	3.7 (3.9)	1.7 (1.6)
	[N,CO]-tt_S(t)	3.4 (3.2)	6.1 (5.9)	1.7 (1.4)	2.4 (3.2)	2.1 (3.4)
	[N,CO]-$tt_S(g_-)$	4.2 (4.1)	7.0 (6.9)	3.5 (3.6)	6.1 (5.9)	6.2 (5.9)
	[CO_2^-]-cc(t)	4.7 (4.2)	4.8 (4.4)	4.8 (4.2)	11.1 (10.6)	16.4 (15.1)
Leu	[N,CO]-$tt_S(tg_+)$	**0.0** (0.3)	1.7 (2.9)	**0.0 (0.0)**	**0.0 (0.0)**	**0.0 (0.0)**
	[CO_2^-]-cc(tg_+)	1.0 (**0.0**)	**0.0 (0.0)**	2.2 (1.0)	6.4 (5.3)	12.6 (10.9)
	[N,CO]-$tt_A(tg_+)$	2.3 (1.5)	3.7 (4.0)	3.5 (2.4)	3.7 (3.9)	1.7 (1.6)
	[N,CO]-$tt_S(g_+g_-)$	3.5 (4.3)	5.6 (7.3)	1.6 (2.0)	2.7 (3.6)	2.3 (3.7)
	[CO_2^-]-cc(tg_-)	3.9 (4.0)	2.7 (3.8)	4.7 (4.5)	8.7 (9.5)	13.9 (13.9)

Ile	$[CO_2^-]$-cc(g_-t)	**0.0 (0.0)**	**0.0 (0.0)**	0.4 (**0.0**)	6.4 (5.0)	12.3 (10.5)
	[N,CO]-tt_S(g_-t)	1.2 (1.8)	3.6 (4.1)	**0.0** (0.1)	**0.0 (0.0)**	**0.0 (0.0)**
	[N,CO]-tt_A(g_-t)	1.6 (1.7)	3.9 (4.0)	2.0 (1.7)	4.2 (3.3)	3.3 (3.0)
	[N,CO]-tt_S(g_+t)	4.1 (4.2)	6.8 (6.9)	2.6 (2.3)	2.9 (3.1)	2.5 (3.0)
	[N,CO]-tt_S(g_+g_+)	4.2 (5.1)	6.7 (7.7)	1.6 (2.2)	2.5 (3.9)	2.6 (5.0)
	$[CO_2^-]$-cc(g_+g_+)	4.2 (3.8)	4.2 (3.8)	3.8 (3.0)	10.1 (8.9)	15.9 (15.9)
	$[CO_2^-]$-cc(g_+t)	5.0 (4.9)	5.1 (5.0)	5.5 (5.0)	11.5 (10.3)	16.3 (10.5)

[a] Ground structure in bold. [b] Calculations performed at the stated level of theory using a 6-311+G(2d,2p) basis set with geometries calculated at B3LYP/6-311+G(d,p) level. [c] Calculations performed at the stated level of theory using a 6-311+G(2d,2p) basis set with geometries and zero-point energies calculated using a 6-311+G(d,p) basis set.

Table 3. Fitting Parameters of Equation 1, Threshold Energies at 0 K, and Entropies of Activation at 1000 K for Cross Sections of the Reactions Indicated[a]

Reaction	Ionic Reactant	Neutral Product	σ_0	n	E_0 (eV)	E_0 (eV) No RRKM	$\Delta S^{\ddagger}_{1000}$ (J/K mol)
$Na^+(Gly) \rightarrow Na^+ + Gly$	[N,CO]-tt	ttt	15.0 (1.5)	1.2 (0.1)	1.70 (0.07)	1.74 (0.07)	47.9 (1.5)
$Na^+(Ala) \rightarrow Na^+ + Ala$	[N,CO]-tt_S	ttt	27.7 (3.4)	1.1 (0.1)	1.73 (0.08)	1.84 (0.08)	50.0 (1.4)
	[CO_2^-]-cc	ttt	27.5 (3.4)	1.1 (0.1)	1.74 (0.08)		49.8 (1.4)
$Na^+(hAla) \rightarrow Na^+ + hAla$	[N,CO]-tt_S(t)	ttt(t)	16.2 (4.4)	1.1 (0.2)	1.74 (0.08)	1.95 (0.09)	50.5 (1.4)
	[CO_2^-]-cc(t)	ttt(t)	16.2 (4.6)	1.1 (0.2)	1.73 (0.08)		48.5 (1.3)
$Na^+(Val) \rightarrow Na^+ + Val$	[N,CO]-$tt_S(g_+)$	ttt(c)	17.3 (3.7)	1.2 (0.1)	1.79 (0.08)	2.17 (0.09)	51.6 (1.4)
	[CO_2^-]-cc(g_+)	ttt(c)	14.9 (3.8)	1.3 (0.2)	1.80 (0.08)		51.9 (1.4)
$Na^+(Leu) \rightarrow Na^+ + Leu$	[N,CO]-$tt_S(tg_+)$	ttt(tg_+)	50.4 (6.5)	1.1 (0.1)	1.80 (0.07)	2.30 (0.07)	54.6 (1.4)
	[CO_2^-]-cc(tg_+)	ttt(tg_+)	48.4 (6.5)	1.1 (0.1)	1.77 (0.07)		49.9 (1.4)
$Na^+(Ile) \rightarrow Na^+ + Ile$	[N,CO]-$tt_S(g_-t)$	ttt(g_-t)	33.0 (4.6)	1.1 (0.2)	1.81 (0.07)	2.31 (0.07)	55.7 (1.4)
	[CO_2^-]-cc(g_-t)	ttt(g_-t)	30.4 (4.4)	1.2 (0.1)	1.76 (0.07)		54.9 (1.3)

[a] Uncertainties (one standard deviation) in parentheses.

Table 4. Enthalpies and Free Energies of Reaction at 0 and 298 K for Na^+–AA Bond Dissociation [a]

Reaction	ΔH_0 [b]	$\Delta H_{298}-\Delta H_0$	ΔH_{298}	$T\Delta S_{298}$ [c]	ΔG_{298}
$Na^+(Gly) \rightarrow Na^+ + Gly$	164.0 (6.9)	2.7 (0.2)	166.7 (7)	34.5 (0.6)	132.2 (7)
$Na^+(Ala) \rightarrow Na^+ + Ala$	167.1 (7.3)	2.6 (0.2)	169.7 (7)	34.7 (0.6)	135.0 (7)
$Na^+(hAla) \rightarrow Na^+ + hAla$	168.1 (7.4)	2.7 (0.2)	170.8 (7)	34.8 (0.6)	136.0 (7)
$Na^+(Val) \rightarrow Na^+ + Val$	172.4 (8.2)	2.6 (0.1)	175.0 (8)	34.5 (0.5)	140.5 (8)
$Na^+(Leu) \rightarrow Na^+ + Leu$	174.1 (6.9)	2.7 (0.2)	176.8 (7)	36.3 (0.6)	140.5 (7)
$Na^+(Ile) \rightarrow Na^+ + Ile$	174.3 (7.0)	2.8 (0.2)	177.1 (7)	36.1 (0.6)	141.0 (7)

[a] Uncertainties in parentheses.

[b] Experimental values from Table 3.

[c] Calculated using standard formulas and molecular constants calculated at the B3LYP/6-311+G(d,p) level.

Table 5. Experimental and Theoretical Na^+–AA Bond Dissociation Energies at 0 K (kJ/mol)

	Experiment				Theory				
AA	TCID[a]	KM[b,c]	KM[c,d]	Eq[c,e]	B3LYP[f]	B3P86[f]	MP2(full)[f]	B3LYP-GD3BJ[g]	M06-2X[g]
Gly	164.0 (6.9)	156 (20)	158 (8)	158 (12)	166.2/*163.3*	161.4/*158.8*	160.3/*151.4*	176.2/*173.3*	169.5/*166.8*
		161	**161**	**160**					
Ala	167.1 (7.3)	162 (20)	164 (8)	166 (12)	172.2/*169.2*	166.4/*163.7*	166.4/*157.0*	183.7/*180.7*	176.9/*173.9*
		167	**167**	**168**					
hAla	168.1 (7.4)	166 (20)			174.7/*171.6*	169.8/*167.0*	169.1/*159.3*	188.4/*185.3*	180.6/*177.7*
		171							
Val	172.4 (8.2)	169 (20)	171 (8)	170 (12)	177.0/*174.1*	172.5/*170.0*	170.8/*160.8*	191.2/*188.0*	183.0/*180.0*
		174	**174**	**172**					
Leu	174.1 (6.9)		172 (8)		177.8/*174.7*	174.0/*171.5*	172.2/*162.7*	191.1/*188.0*	181.7/*178.8*
			175						
Ile	174.3 (7.0)		173 (8)		179.4/*176.2*	174.4/*171.5*	173.2/*162.9*	193.3/*190.0*	185.3/*182.3*
			176						
MAD[h]		5 (3)	3 (2)	3 (3)	5 (2) / *2 (1)*	1 (1) / *3 (1)*	2 (1) / *11 (1)*	17 (3) / *14 (3)*	9 (2) / *7 (3)*
		2 (2)	**1 (1)**	**2 (2)**					

[a] TCID experimental values from Table 3. Uncertainties in parentheses. [b] Kinetic method, Bojesen and coworkers, Ref. [11]. [c] Converted to 0 K values using the enthalpy changes from Table 4. Values in bold have been reanchored here. [d] Kinetic method, Kish et al. Ref. [16]. [e] Equilibrium, Gapeev and Dunbar, Ref. [15]. [f] Calculations performed at the B3LYP, B3P86, or MP2(full)/6-311+G(2d,2p)// B3LYP/6-311+G(d,p) level, ZPE corrections included. Values in italics include BSSE corrections. [g] Calculations performed at the stated level /6-311+G(2d,2p)//Level/6-311+G(d,p) level, ZPE corrections included. Values in italics include BSSE corrections. [h] Calculated mean absolute deviations (MADs) from TCID experimental values. Values in bold provide MADs for relative values.

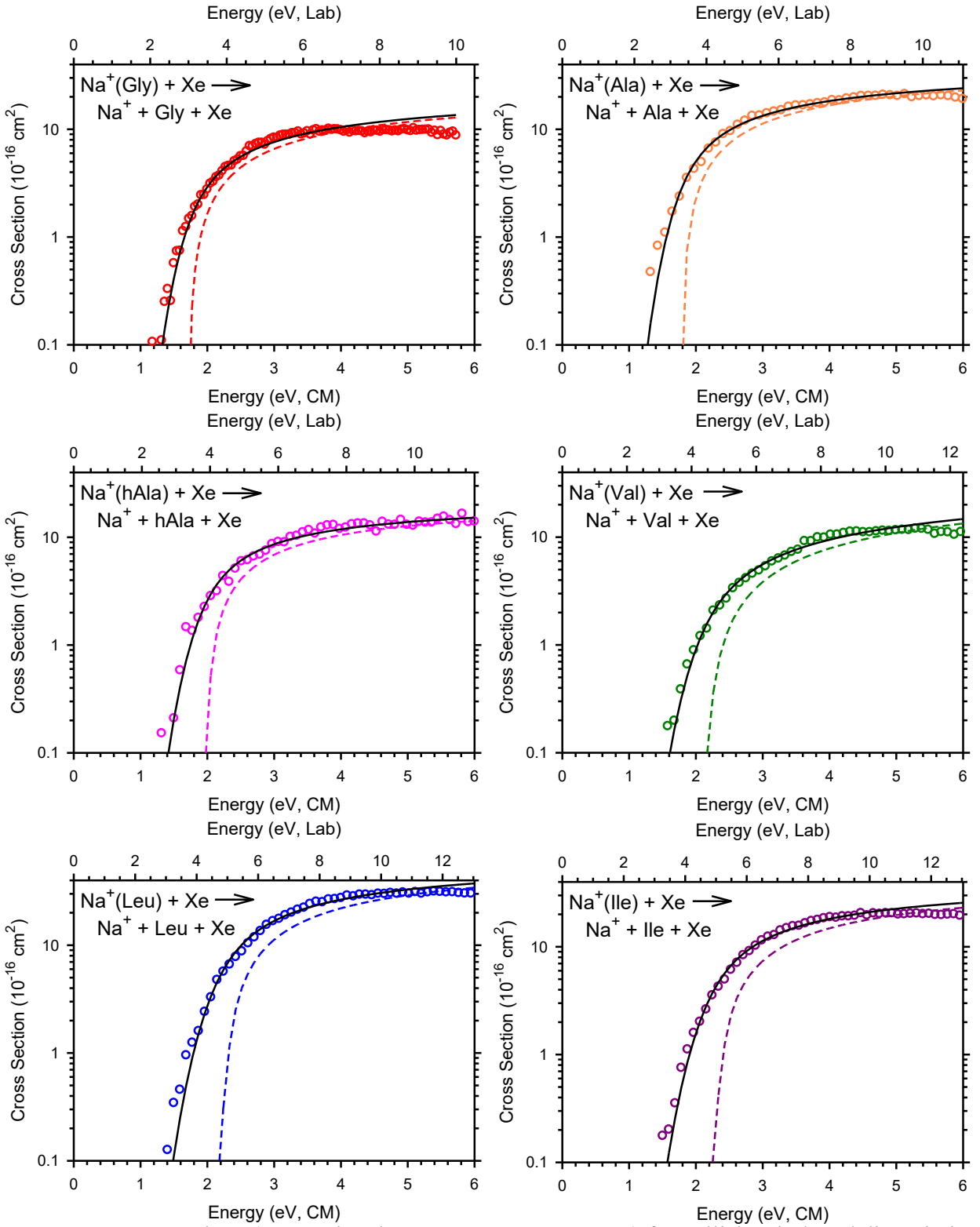

Figure 1. Cross sections (extrapolated to zero pressure, see text) for collision-induced dissociation of Na^+(AA), where AA = Gly, Ala, hAla, Val, Leu and Ile, with Xe as a function of kinetic energy in the center-of-mass frame (lower *x*-axis) and the laboratory frame (upper *x*-axis). Solid (dashed) lines show the best model of the data using eq 1 with (without) convolution over the neutral and ion kinetic and internal energy distributions.

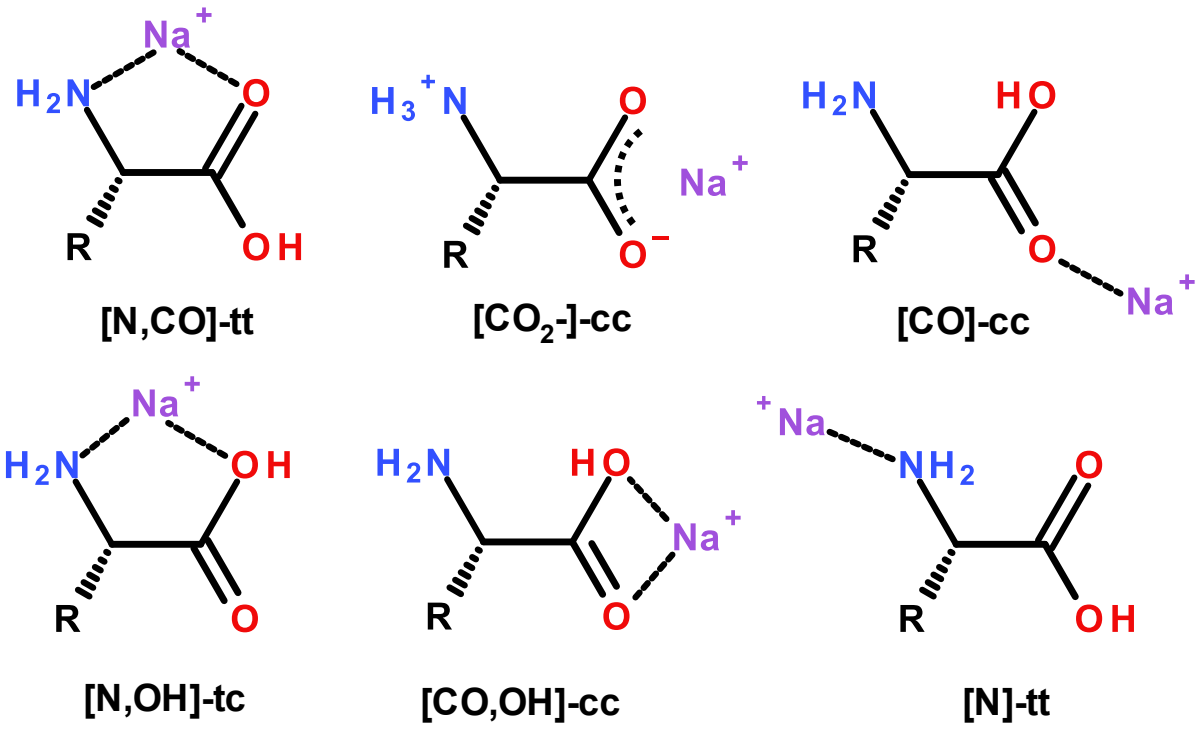

Figure 2. Possible binding modes between Na^+ and aliphatic amino acids where AA = Gly (R = H), Ala (R = CH_3), hAla (R = CH_2CH_3) Val (R = $CH(CH_3)_2$, Leu (R = $CH_2CH(CH_3)_2$, and Ile (R = $CH(CH_3)CH_2CH_3$). See text for a description of the nomenclature.

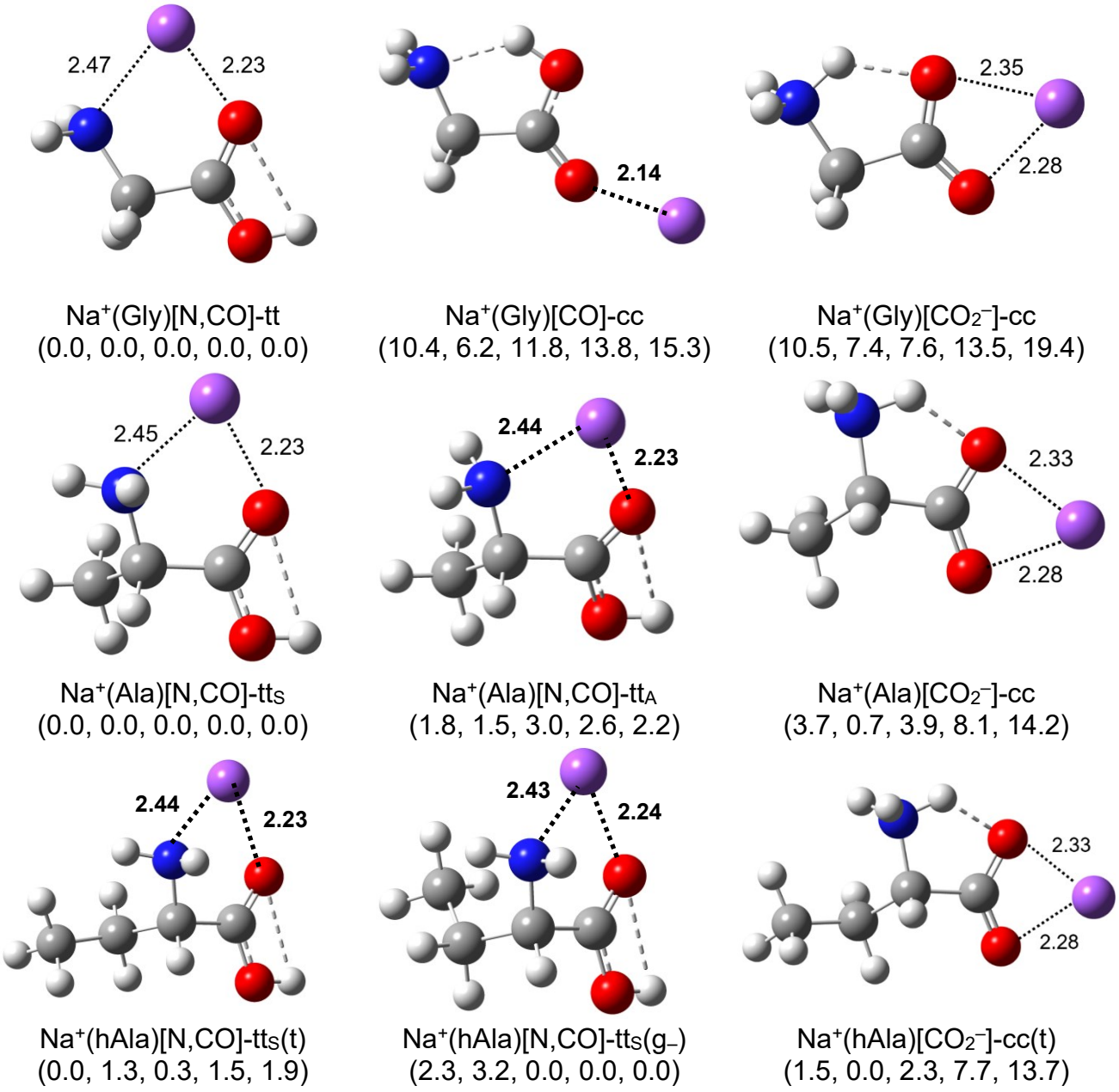

Figure 3. Low-energy structures of Na^+(AA), AA = Gly, Ala, hAla, calculated at the B3LYP/6-311+G(d,p) level. Hydrogen bonds are given by grey dashed lines. Metal-ligand interactions (distances in Å) are given by black dotted lines. Relative energies (kJ/mol) at 0 K from Table 2 are indicated at the B3LYP, B3P86, MP2(full), B3LYP-GD3BJ, and M06-2X levels of theory, respectively.

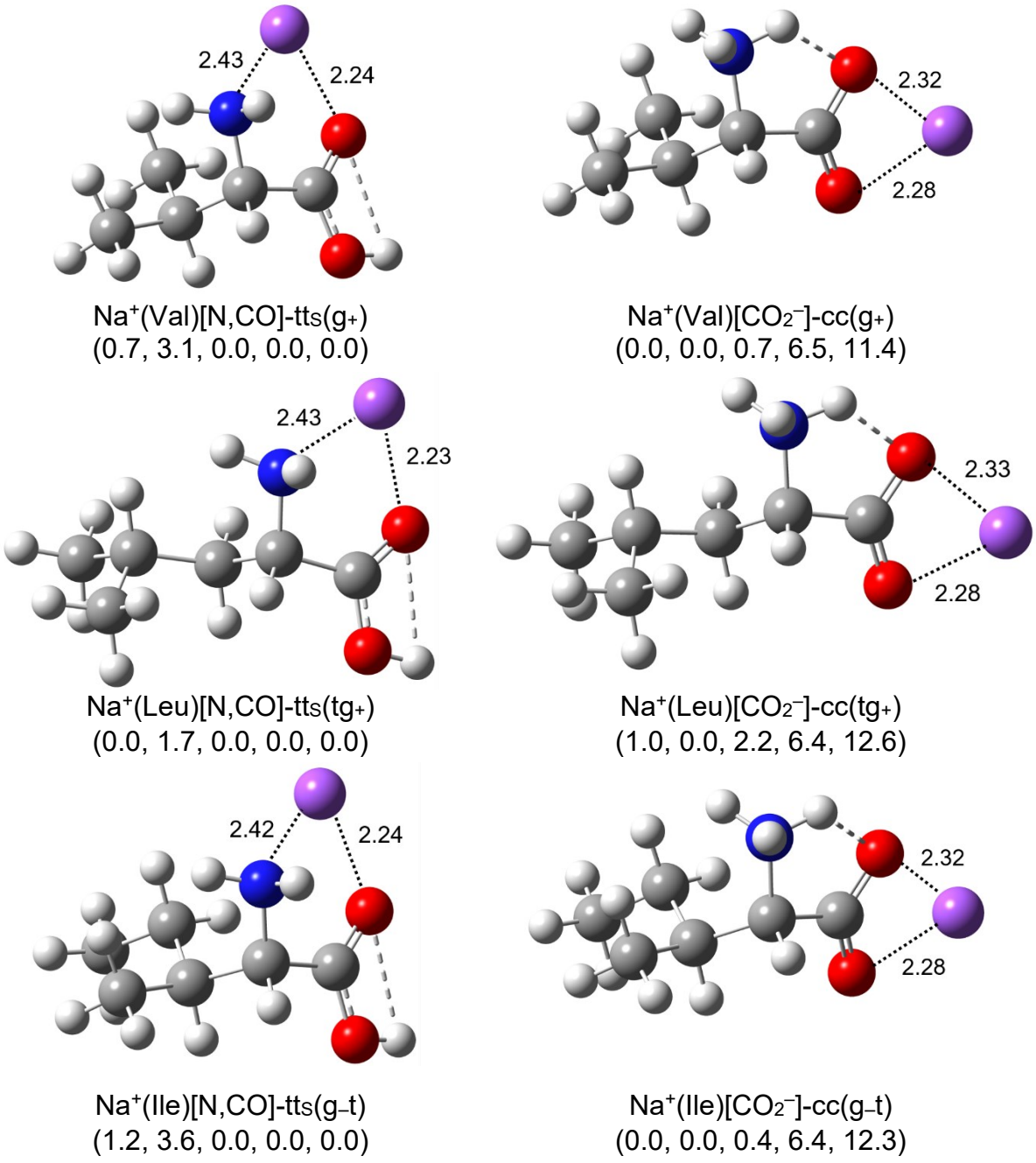

Figure 4. Low-energy [N,CO] and [CO_2^-] type structures of Na^+(AA), AA = Val, Leu, and Ile, calculated at the B3LYP/6-311+G(d,p) level. Hydrogen bonds are given by grey dashed lines. Metal-ligand interactions (distances in Å) are given by black dotted lines. Relative energies (kJ/mol) at 0 K from Table 2 are indicated at the B3LYP, B3P86, MP2(full), B3LYP-GD3BJ, and M06-2X levels of theory, respectively.

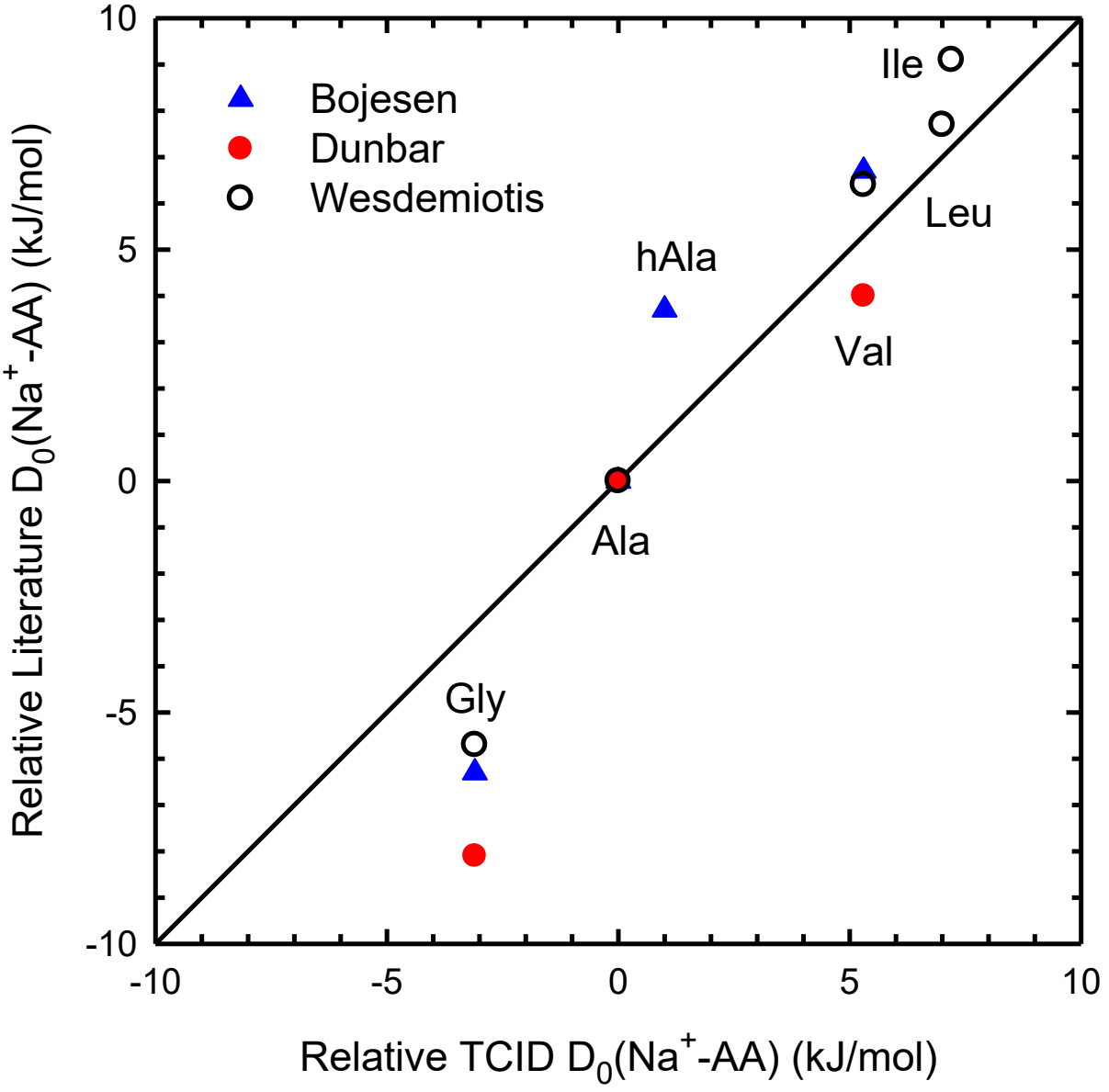

Figure 5. Experimentally determined bond dissociation energies (in kJ/mol) for the dissociation of Na^+(AA), where AA = Gly, Ala, hAla, Val, Leu, and Ile, relative to Ala determined using TCID (x-axis) and the literature (y-axis) from Bojesen et al. (ref. [11], blue triangles), Gapeev and Dunbar (ref. [15], red solid circles), and Wesdemiotis and co-workers (ref. [16], black open circles).

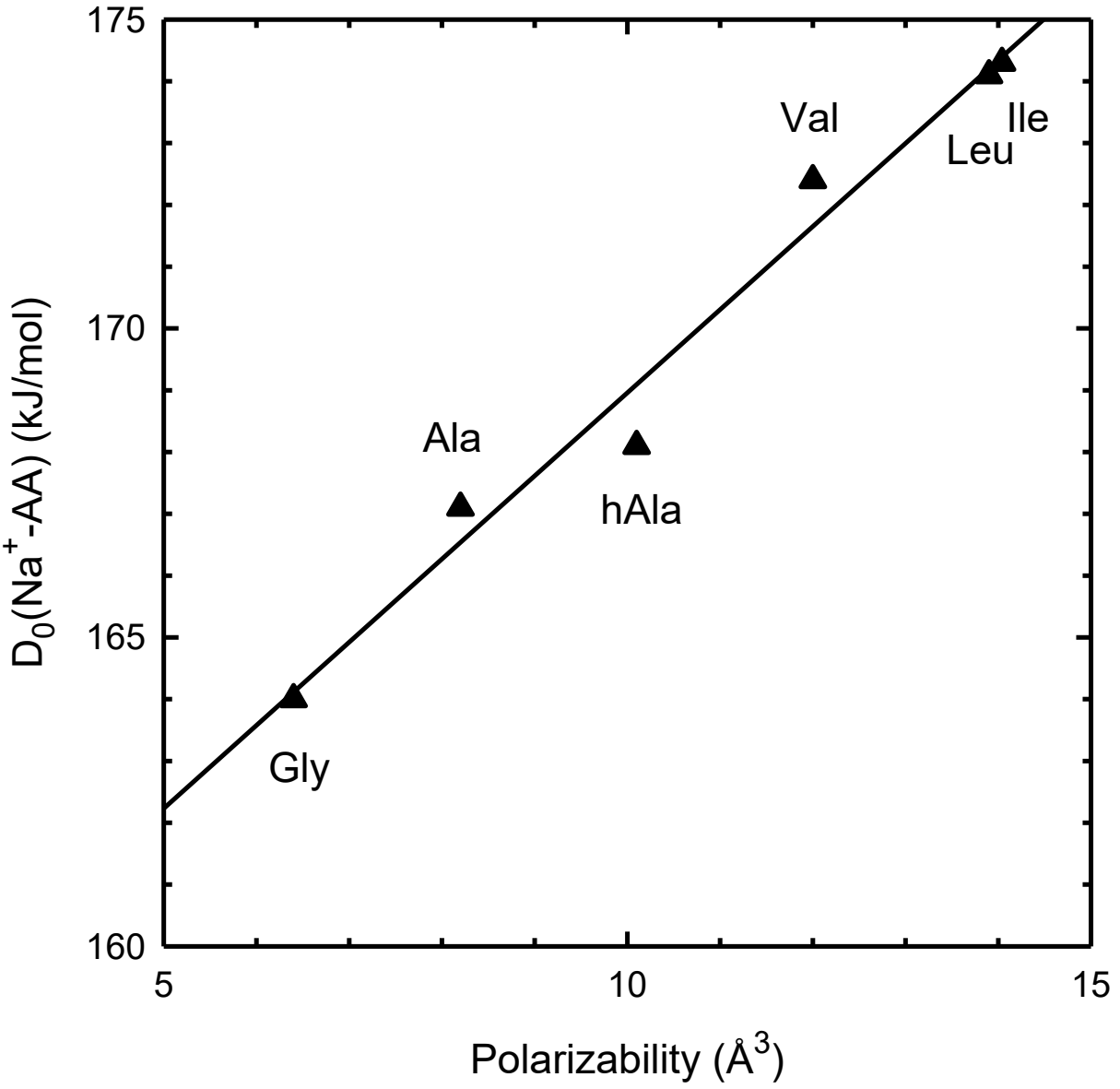

Figure 6. TCID experimentally determined bond dissociation energies (in kJ/mol) for the dissociation of Na^+(AA), where AA = Gly, Ala, hAla, Val, Leu, and Ile, versus AA polarizabilities (Å^3). The line is a linear regression fit to the data described in the text.

TOC Graphic